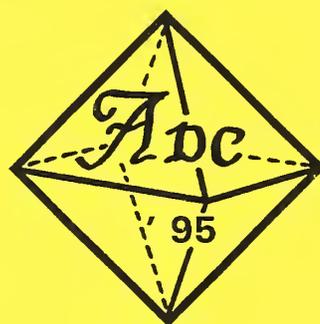**NISTIR 5692**

Supplement to NIST Special Publication 885

Applications of Diamond Films and Related Materials: Third International Conference

A. Feldman
Y. Tzeng
W. A. Yarbrough
M. Yoshikawa
M. Murakawa
(Editors)

Proceedings of the
Applied Diamond Conference 1995

Applications of Diamond Films and Related Materials: Third International Conference

National Institute of Standards and Technology
Gaithersburg, MD
August 21-24, 1995

Edited by

Albert Feldman
National Institute of Standards
*   and Technology*
Gaithersburg, MD, USA

Yonhua Tzeng
Auburn University
Auburn, AL, USA

Walter A. Yarbrough
Pennsylvania State University
University Park, PA, USA

Masanori Yoshikawa
Tokyo Institute of Technology
Tokyo, Japan

Masao Murakawa
Nippon Institute of Technology
Saitama, Japan

APPLIED DIAMOND CONFERENCE 1995

Held at

National Institute of Standards and Technology
Gaithersburg, MD
August 21–24, 1995

Sponsor

National Institute of Standards and Technology

Cosponsors

American Physical Society
Diamond Microelectronics Corporation
Materials Research Society

Cooperating Societies

American Carbon Society
American Ceramic Society
ASM International
IEEE—Electron Devices Society
Japan New Diamond Forum
Optical Society of America
SPIE

TABLE OF CONTENTS

EXAMINATION OF DIAMOND FILM DETERIORATION USING UV RAMAN SPECTROSCOPY

Richard W. Bormett[1], Sanford A. Asher[1], Joyce Birch[2], Robert Lizewski[2], Fred Pettit[2], Robert Witkowski[3], William D. Partlow[3], Aharon K. Inspektor[4] and Edward Oles[4]

[1]University of Pittsburgh, Department of Chemistry, Pittsburgh, PA 15260 USA
[2]University of Pittsburgh, Materials Research Center, Pittsburgh, PA 15261 USA
[3]Westinghouse Science and Technology Center, Pittsburgh, PA 15235 USA
[4]Kennametal Inc., Latrobe, PA 15650 USA

Abstract

UV Raman spectroscopy (UVRS) and SEM are used to determine the type and quantity of nondiamond carbon in CVD diamond films. In addition, we examined degradation of CVD diamond coated and conventional polycrystalline diamond (PCD) tool inserts in the metal cutting environment and compared this degradation to that in oxidizing environments at elevated temperatures. The UVRS measurements show that the cutting process decreases the relative intensity of diamond to nondiamond carbon Raman bands. In contrast, oxidation of CVD diamond films increases the relative intensity of diamond to nondiamond carbon bands.

1. Introduction

Diamond films can now be produced by a variety of chemical and physical vapor deposition techniques. The extent to which these diamond films have the classic desirable diamond properties of hardness and thermal conductivity depends on the type and quantity of nondiamond impurities in the diamond films. We previously demonstrated that UVRS is ideal for characterizing the CVD diamond structure and sensitively monitors graphitic and amorphous carbon impurities[1]. UVRS spectra excited within diamond band gap (230 nm) are fluorescence free and show distinct bands for different nondiamond carbon microstructures. We have used UVRS and SEM to monitor diamond films on cutting tools and have examined the oxidation of CVD diamond films at elevated temperatures. High temperature oxidation preferentially etches away nondiamond carbon at CVD diamond surface, while machining increases the amount of nondiamond carbon on the conventional PCD tools.

2. UV Raman Spectroscopy of Diamond and Nondiamond Carbon

The 228.9 nm excited UVRS of natural diamond, HOPG, microcrystalline graphite and glassy carbon(GC 20) are shown in Fig. 1. Fig. 1a shows the UVRS of polished type IIa diamond. The spectrum can be separated into three regions based on the number of phonons involved in the scattering process. The first order phonon spectrum results from the scattering of a single optical phonon at the maximum in the density of states function of diamond. This 1332 cm^{-1} triply degenerate band is the only allowed Raman fundamental band. Two phonon scattering in diamond which produces a complex band with a maximum at 2467 cm^{-1} and a sharp cutoff at 2667 cm^{-1} consists primarily of overtone and combination bands of phonons at high symmetry points in the Brillouin zone. Careful measurement of the second order phonon spectrum allows accurate determination of phonon energies and symmetries of high symmetry points and critical points in the Brillouin zone. The UVRS second order phonon spectrum of diamond is ten-fold stronger than for visible excitation.

CVD diamond often contains appreciable amounts of nondiamond carbon which exhibit Raman bands characteristic of graphite or highly disordered sp^2 and sp^3 carbon. The first order 1582 cm^{-1} phonon band (G band) of graphite and glassy carbon with 228.9 nm excitation is shown in Figs. 1b-1d. The G band results from an in-plane graphite vibration of E_{2g} symmetry. The graphite Raman spectrum is strongly affected by graphitic ordering. Absent from the 228.9 nm excited Raman spectra of graphite materials is the D band at ca. 1355 cm^{-1} and D band overtones (2450 cm^{-1}, 2710 cm^{-1}, and 2945 cm^{-1}). Since the D bands from graphitic carbon do not appear in the UVRS the diamond first and second order bands are easily measured without interference even for poor quality CVD diamond films with relatively high nondiamond concentrations. The UVRS excited second order spectra of HOPG, and microcrystalline graphite show the 3175 cm^{-1} G band overtone and the 3250 cm^{-1} overtone of a Raman forbidden band (ca. 1620 cm^{-1}). The UV second order spectrum of glassy carbon shows only a broad single band for the 3175 cm^{-1} and 3250 cm^{-1} overtones. The absence of the graphite D band overtones with UV excitation allows the diamond second order phonon band (2467 cm^{-1}) and the carbon-hydrogen (C-H) stretching bands of nondiamond carbon (ca. 2930 cm^{-1}) to be monitored in CVD diamond films.

3. Degradation of Diamond Films at Elevated Temperatures

Figs. 2a and 3a show the SEM of the growth and substrate side (molybdenum substrate) of a diamond film grown via the D.C. plasma torch method (CH_4 - H_2 - O_2 gas mixture). The growth side has crystal facets with geometries indicating (111) and (100) faces. The substrate side has grains with hexagonal shapes and shows voids that develop as neighboring grains impinge upon one another. CVD diamond films oxidize in oxygen environments at temperatures above 400°C. The oxidation rates are extremely rapid at 700°C but decrease to zero at 400°C. Figs. 2b and 3b show SEM micrographs of the growth and substrate sides of the CVD diamond after 5 minutes at 700°C in an oxygen environment. Initial oxidation occurs at grain boundaries and the (111) faces.

Fig. 4 shows the UVRS measurements of the growth side of a CVD diamond film with 0, 2, 4, and 8 minutes of oxidation. The UVRS measurements show that the nondiamond species with bands at ca. 1575 and 2950 and 3100 cm^{-1} are preferentially removed. The diamond second order band at 2460 cm^{-1} also shows a relative intensity decrease compared to the first order diamond phonon band after long oxidation times. This decrease may result from changes in the dominant diamond crystallite orientation. Since the first and second order bands of diamond are strongly polarized, the preferential oxidation of a particular diamond growth surface could lead to an apparent decrease in their relative intensities.

4. Degradation of Diamond During Machining

Figs. 5 and 6 show SEM micrographs of the PCD tool and the CVD diamond coated tungsten carbide-cobalt tools after 4 minutes of machining. Part of the CVD film is completely worn to the substrate (region 1, Fig. 6A). Figs. 5B and 6B show film areas where the diamond is only partially abraided (Fig 5A region 1, Fig. 6A region 2). Fig. 7 shows the 228.9 nm excited UVRS of the PCD tool 200 μm below the cutting edge where the diamond is abraided. Fig. 8 shows the integrated Raman intensity ratio of the diamond first order band to the nondiamond band at ca. 1580 cm^{-1} as a function of distance from the top edge of the tool inserts for a 35 μm probe laser beam. The ratio before cutting was ca. 52 for the PCD tool and ca. 34 for the CVD diamond coated tool.

The relative amount of nondiamond carbon at the PCD tool surface increases after cutting in the abraided and unabraided areas. A large decrease occurs in the diamond band intensity in the exposed area of the CVD diamond tool.

5. References

1. R.W. Bormett, S.A. Asher, R.E. Witkowski, W.D. Partlow, R. Lizewski, and F. Pettit
   J. Appl. Phys. **77**, xxx (1995).

6. Figures
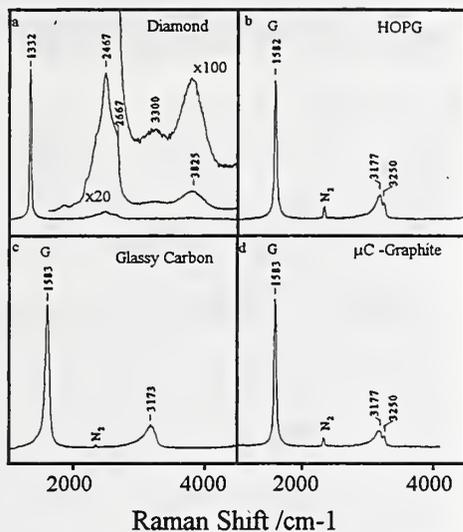
Figure 1. 228.9 nm excited Raman spectra of a) gem quality diamond, b) highly order pyrolytic graphite, c) GC 20 glassy carbon, d) micro-crystalline graphite (< 1 um).
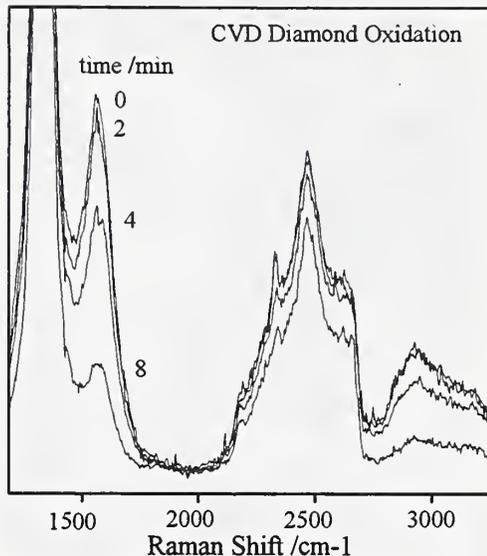
Figure 4. 228.9 nm excited Raman spectra of DC plasma torch grown CVD diamond film after oxidation for 0, 2, 4, 8 minutes in a pure oxygen atmosphere at 600 C.
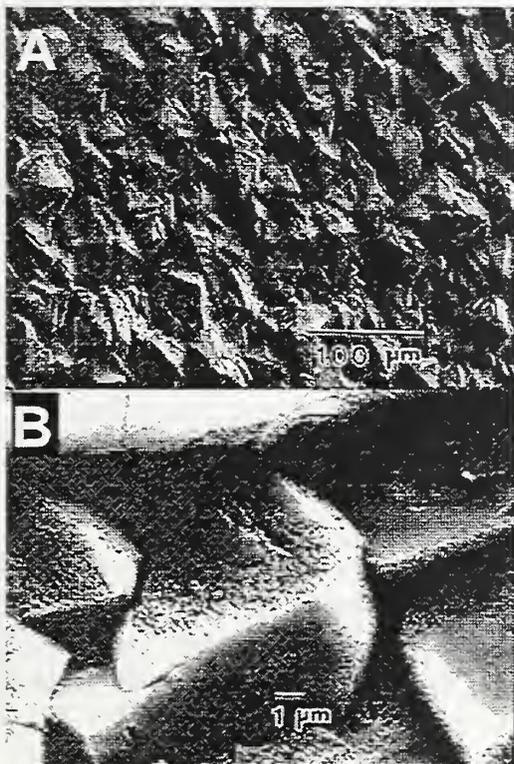
Figure 2. Surface of DC plasma torch grown CVD film before (top) and after (bottom) oxidation.
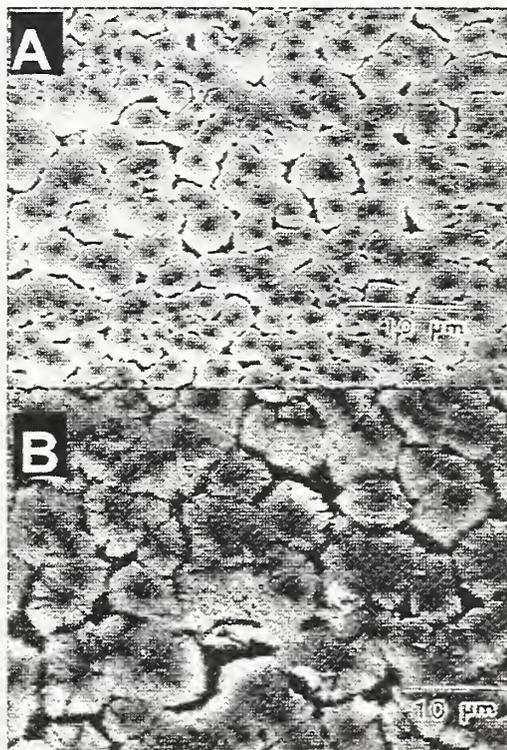
Figure 3. Subsrtrate side of DC plasma torch grown CVD film before (top) and after (bottom)oxidation.

3s
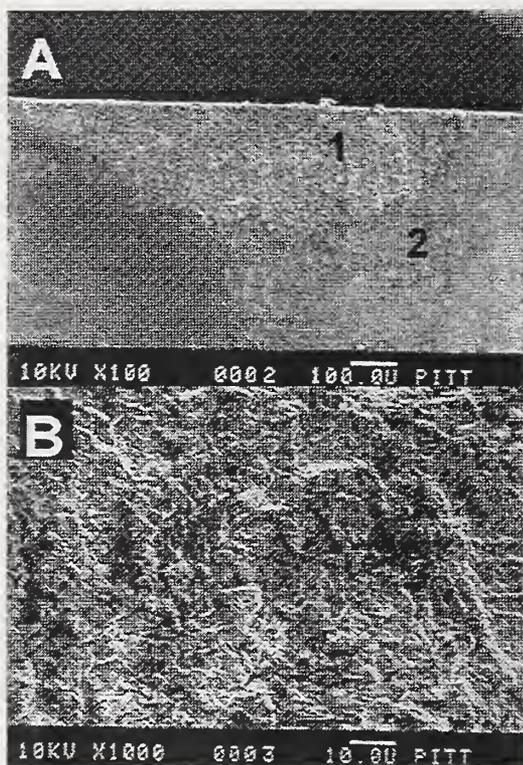
Figure 5. SEM micrograph of PCD tool A) full corner (1) abraided area, (2) unabraided area. B) Abraided area (1) of the wear scar 200μm below the top edge.
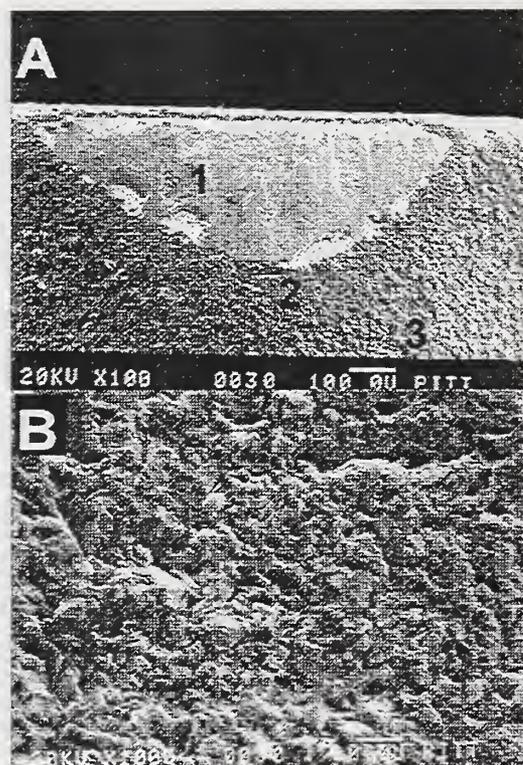
Figure 6. SEM micrograph of CVD coated diamond insert: A) full corner (1) exposed carbide, (2) abraided area, (3) unabraided area. B) Abraided wear area (2) .
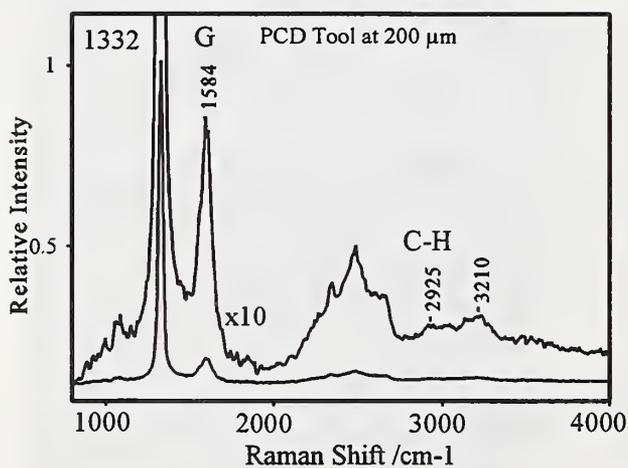
Figure 7. 228.9 nm excited Raman spectrum of PCD tool with 10 sec accumulation and 14 mW.
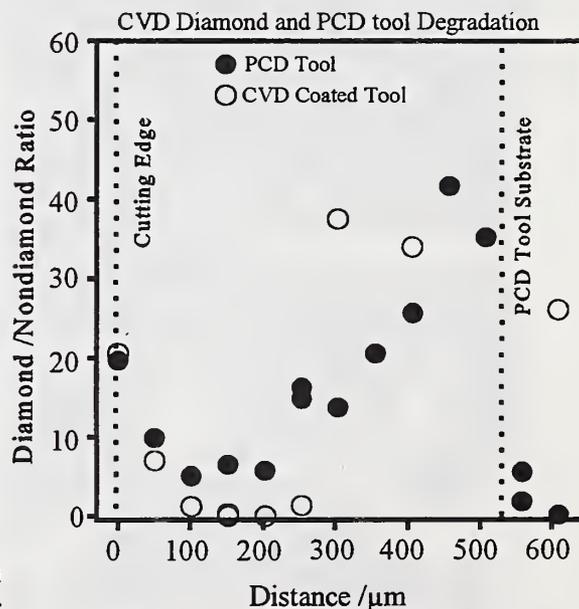
Figure 8. Ratio of integrated peak areas of the 1332cm^{-1} diamond band to the nondiamond band at ca. 1585 cm^{-1}.

STRUCTURAL AND PHASE ORDERING UNDER NON-EQUILIBRIUM SI-C ALLOYS SYNTHESIS.

Kazak-Kazakevich A.Z., Luchinin V.V.

Microtechnology Center, Pr.Popov str. 5, St.-Petersburg, 197376, Russia

Key words: alloys, diffraction, structure, annealing

Abstract

Chemical and structural ordering in amorphous silicon-carbon alloys was investigated using THEED. Si_xC_{1-x} films were prepared by magnetron sputtering, some of them were thermally annealed. Value of x was changed in the range 0.4÷0.6. Substrates temperature under the deposition varied from 300 to 633K. There were obtained the parts of C-C, Si-Si, Si-C chemical bonds and the nearest order was estimated. Deposition temperature 633K resulted to microcrystalline stucture (l<1.5nm). Thermal annealing was carried out under the temperatures 773, 1073 and 1273K. It was found that annealed structure of Si_xC_{1-x} samples strongly depends on the initial chemical order. Initially disordered structures revealed tendency to form cubic packing comparing with chemically ordered ones.

1. Introduction

Structure and properties of a-SiC were investigated in the number of works. It was found tetrahedral structure of a-SiC:H [1,2] with the heterogeneous order predominance. A bond length in a-SiC:H has been found to be 0.186 nm., that is less then corresponding value in crystalline SiC (0.189 nm.). Hygrogen inclusion has nfluence on the properties of SiC alloys [3] including it's structure. Crystalline SiC is known as material forming a wide range of structural modifications, from cubic (3C-SiC) to hexagonal (2H-SiC) [4]. It is of interest, therefore, investigation of the nearest packing type in SiC alloys in the correlation with it synthesis conditions. Chemical and structural state of a-SiC is a subject of interest, especially its numerical characteristics.

2. Experimental section

Films of a-SiC were obtained using method of magnetron sputtering similar to [5]. Film composition was controled by target content and determined using AES-measurements. The temperature of synthesis varied from 300 to 633K, a thickness of the films was 30-40 nm. The layers were deposited on the NaCl substrates then

samples for THEED investigation were easily prepared by means of films separation from substrates in the distilled water.

An intensity distribution of scattering electrons was obtained by means an automatized electron diffractometer EMR-102 at the acceleration voltage equal to 75 kV. Wave number range was 5-210 nm^{-1}. RDFs were calculated according improved technique taking into account multiple scattering effect [6]. Statistical error of the diffraction experiment was 0.22%. Nonelastic electrons were eliminated using electrostatical filter.

3. Results and discussion

Curves of RDFs, corresponding to the stoihometric composition samples of a-Si_xC_{1-x} (x=0.5) are shown in the fig.1. The contributions of the different chemical bonds were found from the RDFs (fig.2) by means of Gauss curves representation. Analysis of radial distribution curves witnesses that higher temperature of a-SiC synthesis leads to a higher degree of chemical and structural order. The first RDF's peak corresponding to Si-C bond (0.189 nm) posseses typical shoulders due to the Si-Si bonds (0.235 nm) and C-C bond (the left and partly the right shoulder). Calculations show that the part of Si-C bonds grows from 62±5% up to 96±4% while temperature changes from 300K to 633K. The tetrahedral structure of a-SiC prevailed already at the room temperature of synthesis. It is made clear by the positions of the two first main RDFs peaks (0.191 nm and 0.309 nm) and the squares under them.

The tetrahedrons are not correlated at the low temperatures of synthesis; the correlation between them is formed only at the deposition temperature T=533K (curve 3, fig.1). The temperature T=633K gives microcrystalline structure with 1.0- 1.5 nm grain dimensions. It was shown that the chemical and structural ordering processes are influenced by composition factor x. So, the chemical ordering was observed to be completed at the x=0.4 or x=0.6 under the T=433K. At the same time the temperature T=633K does not lead to microcrystalline structure in this case. One should note that five times changing the deposition speed does not influence the resulting structure.

Thermal annealing was carried out in tne vacuum at the temperatures 773, 1073 and 1273K during 20 minutes. There were used both kind of samples deposited at the T=300K and 533K. The corresponding RDFs are presented in the fig. 3,4. The processes of chemical and structural ordering were observed, the lower depositing temperature, the more activity of such evolution. 1073K annealing leads to microcrystalline structure (l<1.5nm). The samples annealed at the 1273K gave separated reflections at THEED patterns, the grain dimensions were estimated as 5.0 nm for the 300K deposited films and 2.0 nm for high temperature layers.
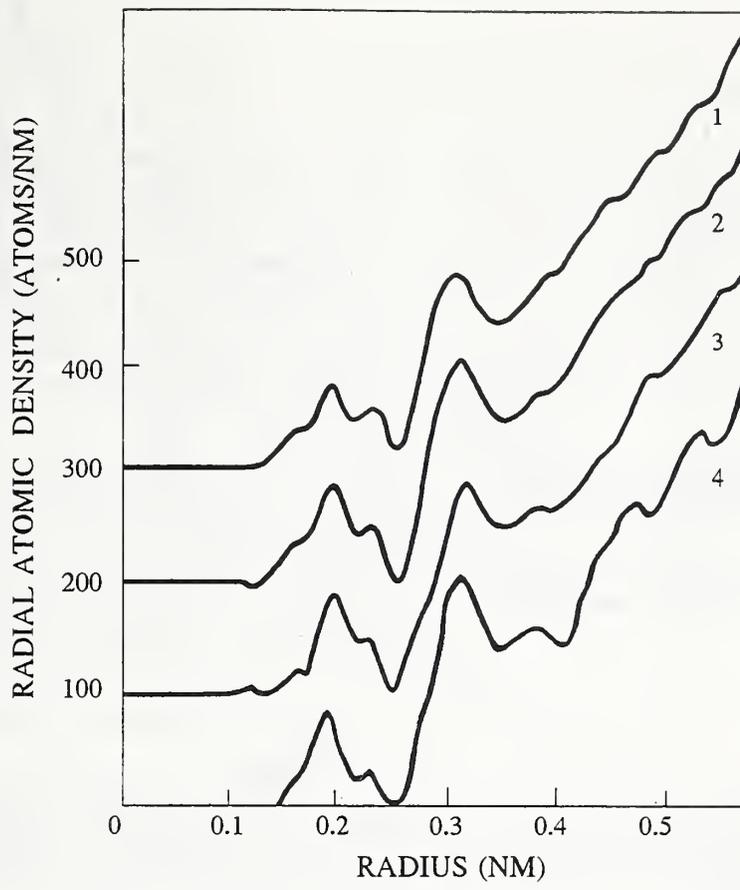
Fig.1 RDFs of Deposited a-SiC Films: 1 - T_s=300K
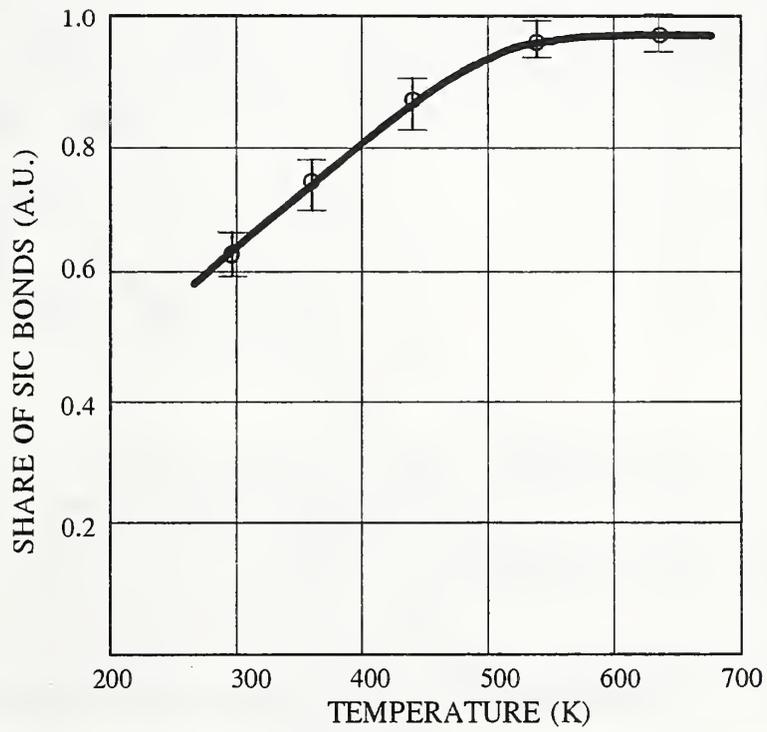2 - T_s=433K; 3 - T_s=533K; 4 - T_s=633K.

Fig.2 Si-C Bonds Share Dependance on the
Temperature of Deposition.
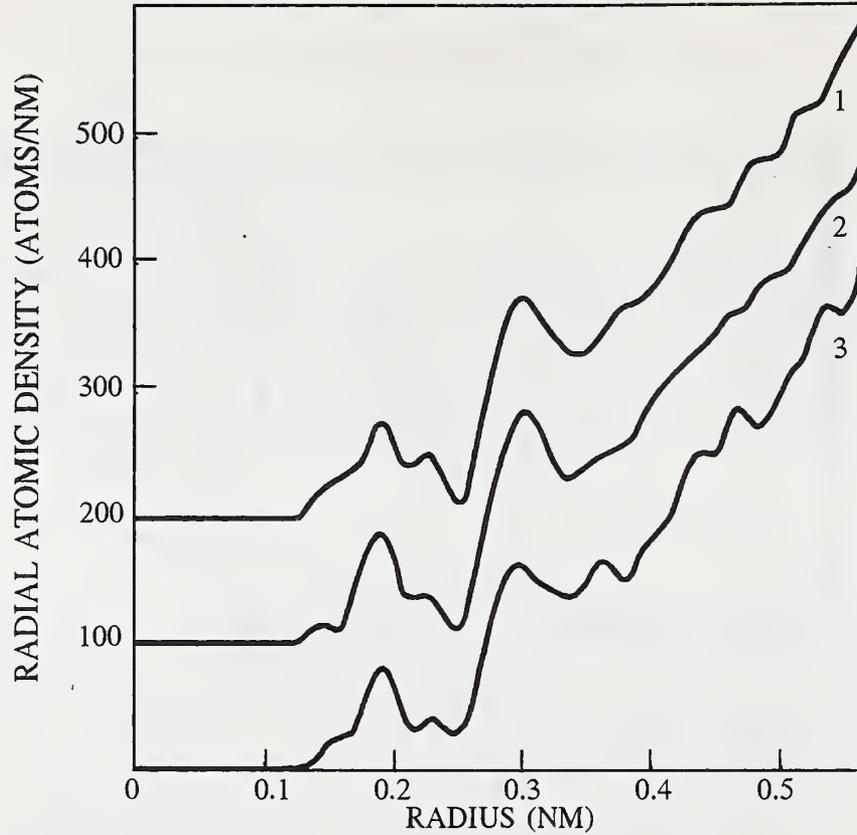
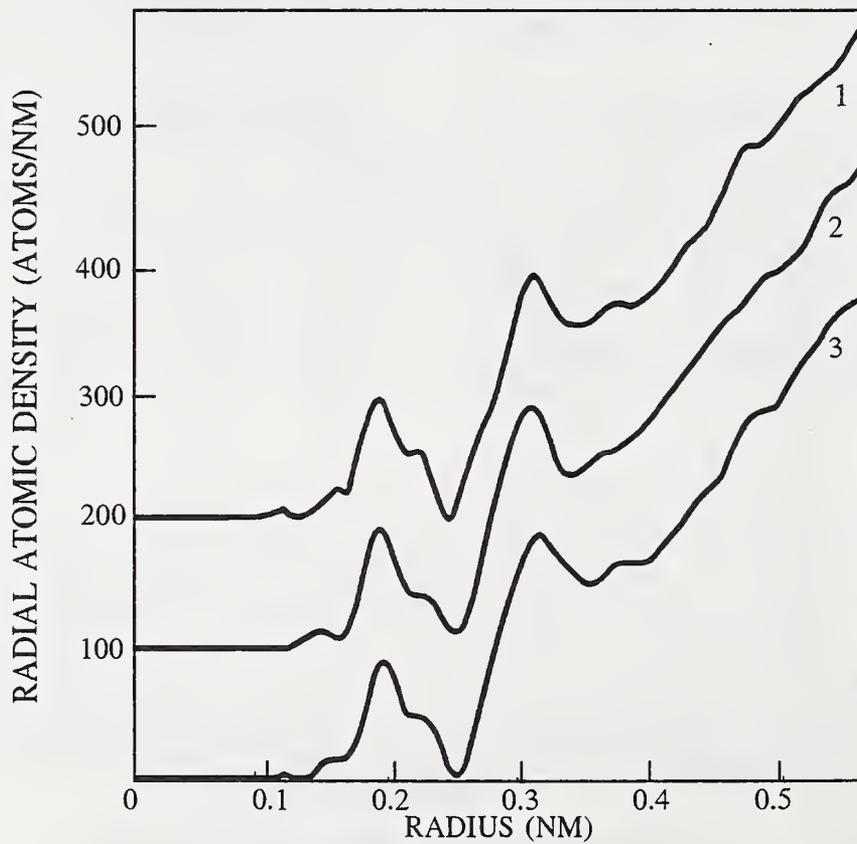Fig.3 RDFs of *a-SiC* Annealed Samples (Temperature of Deposition T_s=300K): 1 - the Initial Structure; 2 - T_a=773K; 3 - T_a=1073K.

Fig.4 RDFs of *a-SiC* Annealed Samples (Temperature of Deposition T_s=533K): 1 - the Initial Structure; 2 - T_a=773K; 3 - T_a=1073K.

Analysis of the nearest ordering type was made using a correlation technique. There were defined the model RDFs corresponding to the 3C and 2H SiC polytypes, then normalized correlation coefficients k between the model function and an experimenal one have been calculated. Calculation revealed more correlation of amorphous SiC with the hexagonal packing then with the cubic one (k_{3C}=0.13, k_{2H}=0.55). At the same time, analysis of the second and third peak squares of the samples deposited under T=633K showed that part of hexagonal packing was not more than 50%.

Investigation of the annealed samples revealed a tendency of hexagonal packing prevalence in a high temperature deposited films, while there took place mostly cubic environment (near 80%) in the annealed samples that had been deposited under T=300K. The tendency was kept at the 1073K annealing. The high temperature deposited samples gave prevalence of 4H, 2H-SiC polytypes, while low temperature deposited samples leaded to 3C, 15R, 6H polytypes.

4. Conclusion

The present investigation showed a good efficiency of improved electron diffraction RDF method to study chemical and structural ordering in the binary system such as a-Si_xC_{1-x}. It has been confirmed the tetrahedral structure of a-SiC in the wide range of synthesis conditions. The paper presents an approach to the nearest packing analyse in a-SiC. It was shown that a-SiC structure mostly correlates with the hexagonal type of packing similar to amorphous silicon, but the increasing of deposition temperature leads to the cubic packing probability increasing. The structure of thermally annealed films revealed clear dependence upon initial chemical and structural order. The lower initial order, the higher resulting structural order as well as probability of cubic packing.

5. Acknowledgment

6. References

1. Makenzie D.R., Smith G.B., Lui Z.O. Electron diffraction study of chemical ordering in glow discharge a-Si_xC_{1-x}:H. - Phys. Rev. B., 1988,Vol.37,N15,p.8875.
2. Pascarelli S., Boscherini F., Mobilo S. The structure of hydrogenated amorphous silicon carbon alloys asinvestigated by EXAFS.- Lab. Naz. Frascatti.[Rapp.]., 1991, N91-012,p.1-8.
3. Demichelis F., Grovini G., Pirri C.F., Tresso T., Giamello E., DellaMea G. Hydrogen evolution in amorphous silicon carbide. Physica B.,170,N1-4,p.149-152.

4. Verma A.R., Krishna P. Polymorphism and polytypism in crystalls. J.Willey, New York, 1966.

5. Wahab Q., Haltman L., Sundgren J.-E., Willander M. Composition and structure of epitaxial β-SiC films grown by reactive magnetron sputteriing on Si(100) substrates: Pap. Eur. Mater. Res. Soc. Fall Meet., Strasbourg, Nov 27-30, 1990/ Mater. Sci and Eng.B.,1992, 11,N1,4, p.61-66.

6. Kazak-Kazakevich A.Z. Radial distribution function method improvement. News of the Leningrad Electrical Engineering Institute, Leningrad, 1991,Issue N433, p.30-35.

EXAMINATION OF ELECTRON FIELD EMISSION EFFICIENCY AND HOMOGENEITY FROM CVD DIAMOND FILMS.

A.T.Rakhimov[1,2], B.V.Seleznev[1,2], N.V.Suetin[1], A.V.Kandidov[1], V.A.Tugarev[1], and I.A.Leont'ev[2].

[1] Institute of Nuclear Physics, Moscow State University, Moscow 119899, Russia.
[2] Digazcrown Inc., 29, Leninskii prospekt, Moscow 117912, Russia.

Key words: diamond, field emission, CVD.

Abstract.

This paper presents the results of the investigation of electron emission efficiency and homogeneity from diamond films. Diamond films were grown by plasma enhanced DC glow discharge method on Si and Mo substrates with the diameter up to 30mm. For the best films the emission "switch-on" threshold is 8V/micron and at 10V/micron the emission current density exceeds $50\mu A/mm^2$.

1. Introduction.

It was stated in a number of recent publications that the surface of diamond and diamond-like films has high efficiency of processes of electron field emission (EFE) [1,2]. The investigation of EFE of such materials was stimulated by the detection of the phenomenon of the negative electron affinity of the diamond surface [3]. However, the true nature of the high emission properties of diamond films (DF) is still unclear and this is the barrier to the development of the high reproducible emitter technology having reasonable spatial homogeneity, low emission threshold and high output. Apparatus for studying DF EFE and some previous results produced in DGC are presented in this report. It was found that our CVD grown DF have homogeneous EFE with low threshold.

2. Emission characteristics measurements.

There are three main parameters that characterise cathode's properties and that provides knowledge on its applicability for display fabrication. These main parameters are:
1. emission efficiency of the cathode that results in the total display brightness,
2. spatial homogeneity of the emission current affecting on the achievable brightness levels,
3. cathodes temporal stability.

To measure first two parameters special apparatus schematically shown on fig.1 is used. Phosphor coated glasses were used as anodes, and the anode-cathode gap was 100 microns typically. Experiments were carried out in vacuum chamber with pressure better than $5*10^{-5}$Torr. Power supply provides pulses of up to $5*10^{3}$V with repetition rate 1-100Hz and pulse duration 1-100μs. Usually we put pulse duration - 30μs and repetition rate - 50Hz, which is close to parameters of real displays. Though for good cathodes pulse duration was reduced to 3μs to prevent phosphor damage.

Emission images of the cathode are recorded by CCD camera and stored in PC for processing. Usually we record emission images of one cathode taken at different values of applied field.
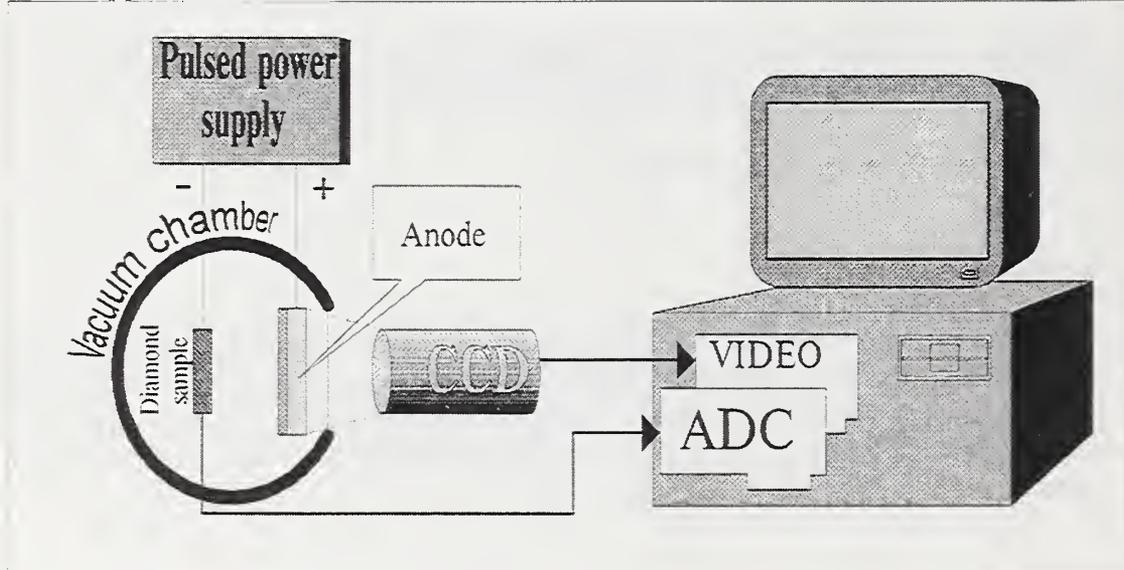
Fig.1. The scheme of the experimental set-up.

The cathode's emission efficiency is characterised by its integral field-current characteristic. The integral field-current characteristics also give knowledge about emission homogeneity. Really, every emission surface consists of a large number of independent emission sites. Every site has its own field-current characteristic with its own "switch-on" threshold. If all emission sites have absolutely the same field-current characteristics, their integral characteristics will have sharp "switch-on" threshold. But as real cathode's emission sites have different field-current characteristics the integral one

12s

has a blurry (washed-out) "switch-on" threshold. So the sharpness of the cathode's integral field-current characteristics gives the knowledge of its emission spatial homogeneity.

Integral field-current characteristic describes homogeneity of emission sites' properties, but does not give the knowledge on their spatial distribution.

The estimation of the spatial distribution of emission sites on the cathodes is obtained from emission images recorded by CCD and treated by specially developed software. This software performs segmentation of the cathode's surface for all further analysis to be done only within cathode's area. It calculates the luminescent area and estimates spatial uniformity of the cathode. So far it becomes possible to plot the dependence of the luminescent area on the applied field and again estimate the "switch-on" field range.

Fig.2a-e illustrate the "emission development" of a part of a typical diamond cathode.

a   b   c   d   e
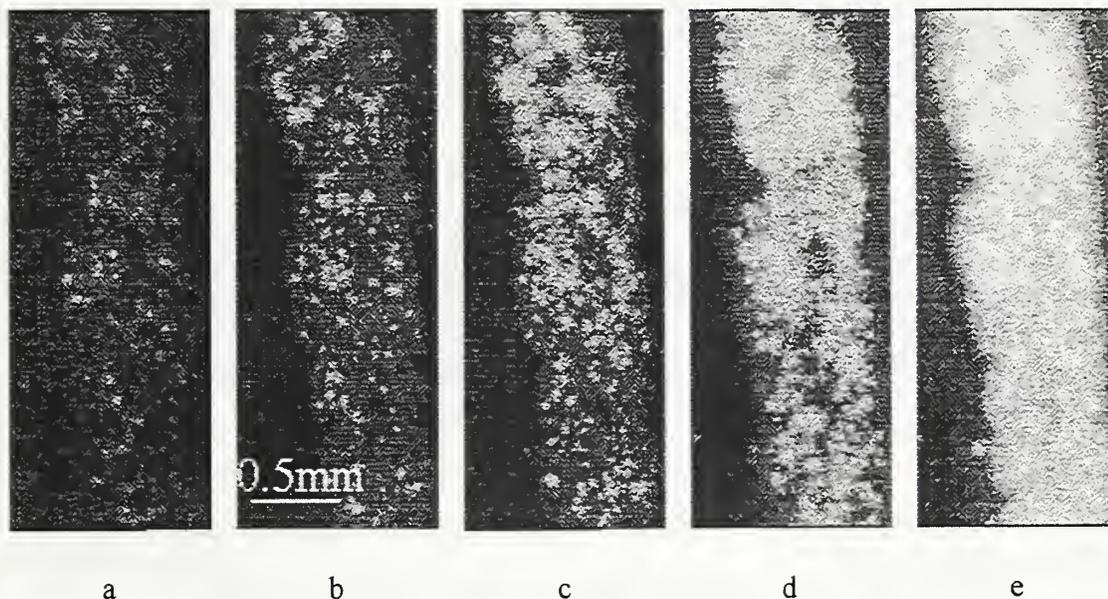
Fig.2. The "emission development" with the increasing of the applied field.(a part of the CVD-grown diamond sample) a-10.4V/μm, b-10.8, c-11.2, d-11.6, e-12.8V/μm.

The integral field-current characteristic of this cathode taken simultaneously with the images is presented on fig.3, and fig.4 presents the dependence of the luminescent phosphor's area on applied field. The marked points on these plots correspond to similarly marked emission images.

We estimated the emission current density from our best films to be about 50μA/mm^2 at 10V/micron and the switch-on threshold range - less than 3V/micron.
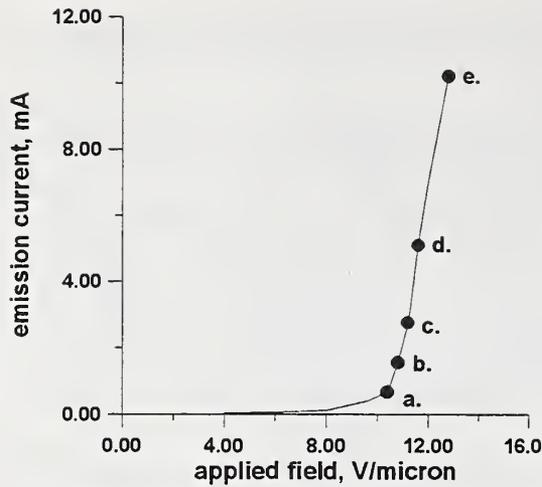
Fig.3 Integral field-current characteristic
of a CVD-grown diamond sample
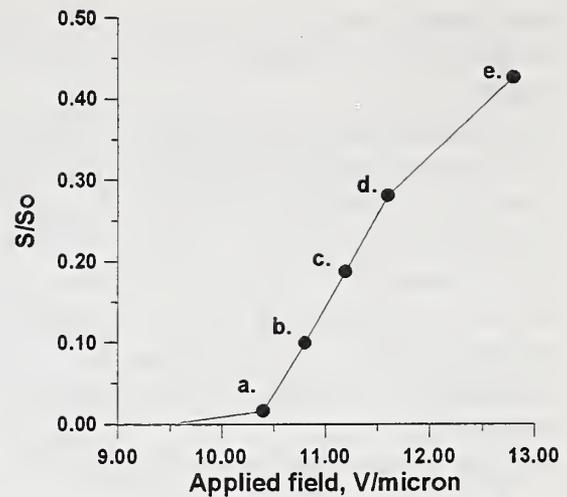
Fig.4 The increase of the phosphor's lu-
minescent area with the increase of the
applied field for a sample's part.

3. Conclusion

Special equipment for investigation of electron field-emission homogeneity and efficiency has been developed. CVD-grown diamond films have been studied by using this equipment. It was found that these films have sufficiently high spatial homogeneity of emission centres, low "switch-on" threshold voltage range and high current density. This shows that CVD-grown diamond films have perspectives for application in flat panel displays.

4. References.

1. C.Xie, N.Kumar, C.B. Collins et. al. Sixth Int.Vacuum Microelectronics Conf., 1993, Newport, p.162
2. N.S. Xu, Y. Tzeng, R.V. Lathman J.Phys. D: Appl. Phys. 26 (1993) 1776
3. F.J. Himpsel et.al. Phys.Rev. B20 (1979) 624

EXPERIMENTAL AND THEORETICAL APPROACH TO CHEMICAL BEAM EPITAXY OF cBN

Shojiro Komatsu and Yoichiro Satoh

National Institute for Research in Inorganic Materials
1-1 Namiki, Tsukuba, Ibaraki 305, Japan

Abstract

Chemical beam epitaxy(CBE) method is introduced to carry out the study of cBN deposition on well-defined surfaces and the in-situ observation of the surfaces using an RHEED(reflection high energy electron diffraction)-TRAXS(total reflection angle X-ray spectroscopy) system[1]. The CBE study is theoretically assisted by semiempirical MO calculations of nanocrystals to model hydrogenated surfaces of cBN[2]. The (100)N was found unique because it stabilizes as fully-hydrogenated dihydride structure. On the other hand, the (100)B was predicted to stabilize as monohydride structure, which is similar to hydrogenated surface of diamond(100). Photo-assisted depassivation of the (100)N is suggested by the spatial distribution of the LUMO.

1. Introduction

Recent progress in UHV (ultra high vacuum) technology for surface science has contributed very much in fundamental studies of molecular beam epitaxy (MBE) of semiconducting materials. There we can use surface-analytic methods using electron beam as in-situ probe of surfaces, because of the low pressure. However, the advanced UHV technology has not yet been commonly applied to studies of chemical vapor deposition(CVD). In particular, vapor deposition of cBN, which often meets difficulty in the reproducibility, seems to need this sort of approach. The difficulty is supposed to partly originate from the undefined surface of the substrates. Experiments using UHV is beneficial since we can prepare well-defined substrate surface prior to deposition by using methods familiarized in surface scientific studies.

We introduce here a new experimental device for chemical beam epitaxy (CBE) of cBN, that is probably the first attempt to apply the high vacuum methodology developed in association with the MBE studies, to the exploration of fundamental problems in cBN deposition.

2. Methods

The CBE method is employed mainly in order to carry out the deposition on well-defined surface of the substrate and in-situ observation of the growing film surface. The main deposition chamber is equipped with an RHEED-TRAXS system for the in-situ observation of the surface structure and composition(Fig.1). Three radical sources are used to generate diborane, ammonia, and hydrogen plasma, respectively, for the deposition. Hot-filament or laser assistance of the CBE process is also available. Single-crystalline diamond and silicon substrates are tried for the deposition. The system could reach 10^{-8} Pa with the assistance of a titanium sublimation pump in addition to a turbo molecular pump and a rotary pump. 5% biborane and ammonia each diluted in Ar are used. The Ar and H_2 gas were 99.9999% purity. Maximum flow rates of the diluted diborane and ammonia, and hydrogen are 10 sccm, respectively. Maximum substrate temperature is 1000 °C. Pressure of 10^{-1} Pa can be realized by using the turbo-molecular pump of 1500L/min at the maximum flow rates of gases in the deposition chamber while the RHEED system is maintained at as low as 10^{-4} Pa by differential pumping.

In view of $(1 \times 1):2H$ dihydride / $(2 \times 1):H$ monohydride reconstruction, structural stability of (100) surfaces of both cBN and diamond was comparatively investigated by semiempirical molecular orbital methods (AM1 and PM3 approximations, respectively) using isoelectric clusters of $B_{52}N_{50}H_{84-2n}^{(2-)}$, $N_{52}B_{50}H_{84-2n}^{(2+)}$, and $C_{102}H_{84-2n}$, to model (100)B and (100)N of cBN, and C(100), respectively, where $n = 0, 1, 2,$ or 3. The n denotes the number of monohydride dimers formed. These clusters were nanometer-sized crystallites bound by {111} faces.

3. Results

The $C_{102}H_{80}$ cluster, bound by {111} surfaces with two monohydride dimers formed at the top ridge as shown in Fig.2, characterizes the common crystallography of the nanocrystals. All of the dangling bonds at the eight {111} surfaces are terminated

with atomic hydrogen. Top ridges of the clusters are used to represent (100) surfaces, where at most three neighboring dimers can reside along [110] direction thereon. The cluster measures about 1.50 nm along the ridge direction.

Figs.3(a), (b), (c) and (d) show the $B_{52}N_{50}H_{84-2n}^{(2+)}$ cluster where n = 0, 1, 2 and 3, respectively.

Fig.4 shows the enthalpy change in the formation of monohydride dimer(s) with hydrogen molecule(s) desorbed. For instance, in the case of diamond, it shows the enthalpy change in the reaction, $C_{102}H_{84} \rightarrow C_{102}H_{84-2n} + nH_2$, where n = 1, 2, and 3. These results are obtained for the clusters at their lowest singlet states. As one monohydride dimer forms, diamond(100) and cBN(100)B surfaces achieve great stabilization by 59 and 76 kcal/mol, respectively, indicating relaxation from the steric repulsion. However, on the other hand, cBN(100)N surface destabilizes by 11 kcal/mol as one monohydride dimer forms. Further progress of monohydride formation makes the destabilization much more in the cBN(100)N surface. These result indicate that the (100)N stabilizes as fully-hydrogenated dihydride structure while the (100)B stabilizes as monohydride structure in a similar manner as diamond(100) does.

4. References

[1] S.Ino, T.Ichikawa and S.Okada, Japan. J. Appl. Phys.19, 1451(1980).
[2]S. Komatsu, W. Yarbrough and Y. Moriyoshi, to be published.
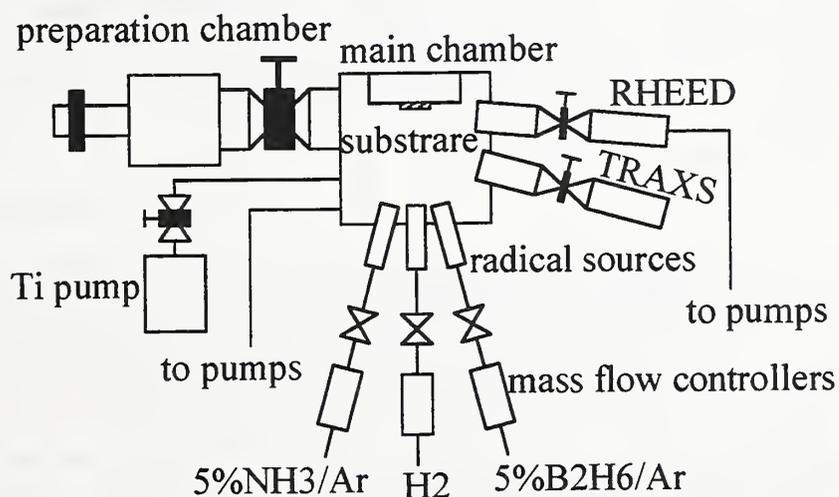
Fig.1 Experimental setup

[110]
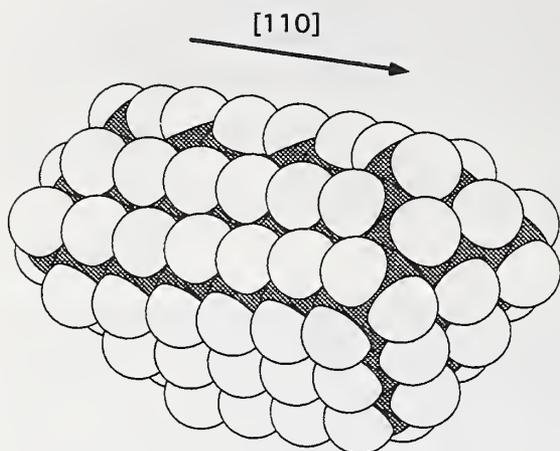
Fig.2 C102H80 cluster
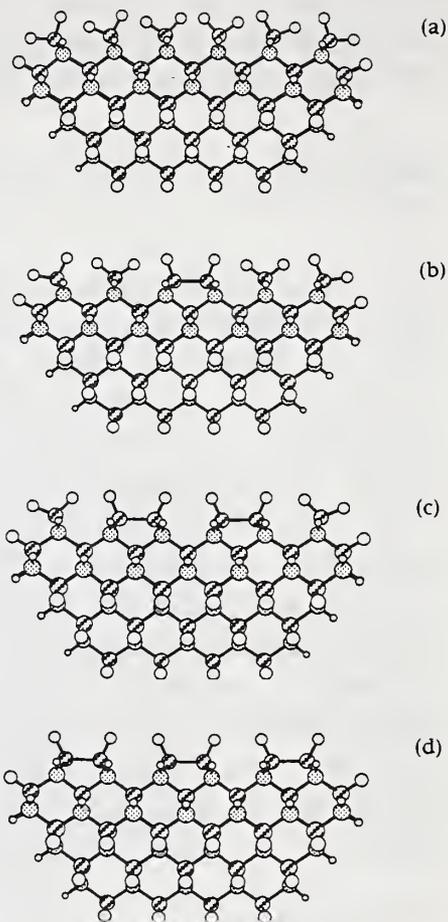
(a)

(b)

(c)

(d)

Fig.3 (a), (b), (c) and (d) show the $B_{52}N_{50}H_{84-2n}^{(2+)}$ cluster where n = 0, 1, 2 and 3, respectively.

Enthalpy change (kcal/mol)

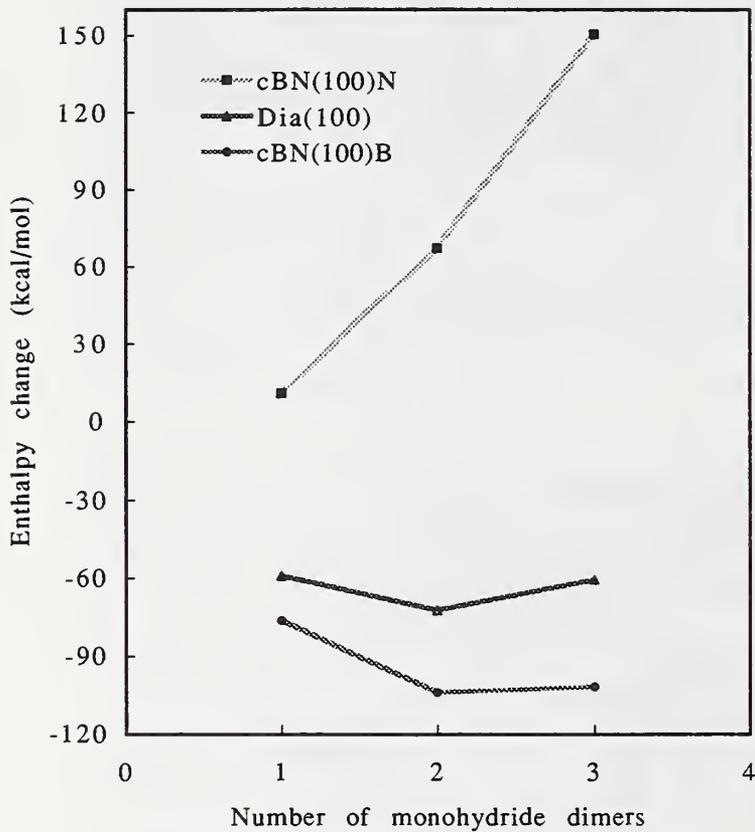Number of monohydride dimers

cBN(100)N
Dia(100)
cBN(100)B

Fig.4 The enthalpy change in the formation of monohydride dimer(s) as hydrogen molecule(s) desorbed.

AMORPHOUS HARD BORON NITRIDE FILMS PREPARED BY PLASMA ENHANCED CHEMICAL VAPOR DEPOSITION

Hidetoshi Saitoh, Jun Satoh, Takashi Ishiguro, Kiichiro Kamata and Yukio Ichinose

Nagaoka University of Technology
Kamitomioka, Nagaoka, Niigata 940-21, Japan

Key words: boron nitride, CVD, plasma, dc bias voltage, Knoop hardness, adhesion

Abstract

Amorphous boron nitride films were prepared on Si substrates by plasma enhanced chemical vapor deposition with a BCl_3-N_2-Ar-H_2 gas mixture. The surface of the resulting films indicated a Knoop hardness of 60000-80000 N/mm^2 at a loading force of 100 mN. Scratching test revealed that the critical load of the boron nitride films was higher than that of diamond like carbon films prepared on Si substrates.

1. Introduction

Recent success in obtaining chemical-vapor-deposited films has presented an approach to hard boron nitride synthesis [1-6]. This approach was originally applied for preparation of hexagonal BN (h-BN). The plasma excitation or filament heating technique which is of assistant to the thermal chemical vapor deposition (CVD) process made it possible to nucleate c-BN with hexagonal material. Although the films, including both hexagonal and cubic BN, show no delaminating or no cracking into flakes, no report has been provided on their mechanical properties due to the extreme difficulty in obtaining rapid growth or thick film. We have designed and constructed a dc and rf plasma CVD apparatus to prepare boron nitride films. 3-µm-thick films were synthesized using this apparatus with a BCl_3-N_2-H_2-Ar gas mixture. These specimens allowed direct evaluation of mechanical properties of CVD-boron nitride because of their relatively large thickness and good adhesion stability. In this article, crystal structure, hardness and adhesion of the films are described and discussed.

2. Experimental procedure

The low pressure boron nitride growth was performed using a plasma CVD reactor. This apparatus consists of an rf plasma spray for Ar+N_2 gas mixture and a electric heater for decomposition of BCl_3. The rf power supply used in this study was a 13.56 MHz rf generator with a maximum power of 500 W. This is coupled to the rf plasma spray through an induction coil. Single crystal wafers of non-doped or p-type Si (100) are initially placed on the electric heater. With this heater the substrate temperature can be heated to 650°C. Negative dc bias voltage is applied to the substrate stage. During processing, the reaction chamber is pumped by an anti-

chemical type rotary pump. The chamber can be evacuated to a base pressure of 1×10^{-2} Torr. The film deposition was performed as follows. The flow rates of BCl_3, N_2, H_2 and Ar were 10, 14, 200 and 136 sccm, the net rf power was maintained at 100 W for 30 min, and the total gas pressure was 2 Torr. The substrate temperature and negative dc bias voltage were varied on each of the experiments.

3. Results and discussion

Figure 1 shows SEM micrographs of deposits synthesized at a substrate temperature of 400°C and a negative bias of 450 V. As indicated in Fig. 1 (a), dendritic aggregations with 3-5 μm in size were seen. They were grown along to the scratched mark as if diamond nucleation on the scratched Si substrate. Cross-sectional observation shown in Fig. 1 (b) reveals that both dendritic aggregation and continuos film are deposited on the substrate. The deposition rate of the continuos film is approximately 6 μm/h, however it slightly decreases with decreasing the substrate temperature and negative bias voltage. All samples showed no surface cracking or peeling, suggesting good adhesion.

The results from Raman scattering spectroscopy and Auger electron spectroscopy, obtained from the substrate temperature series, confirm that deposits are boron nitride having surface contamination including carbon and oxygen. Typical microfocus Raman spectra emitted from dendritic aggregation are shown in Fig. 2. A Raman peak at 1367 cm⁻¹ was obtained from the samples deposited at temperature ranging 400-500°C. Following previous assignments [7], h-BN exhibits two symmetry-allowed vibrational mode of E_{1u} symmetry at 1367 cm⁻¹ and a rather low frequency (<150 cm⁻¹). Although the lesser one was not detected due to out of range on our spectrometer, the resulting peak suggests the presence of h-BN. In contrast, no Raman peak was obtained from continuos films on all samples.

There is direct evidence of boron nitride growth on Auger electron spectra as shown in Fig. 3. Peak intensity ratios of B and N main peaks decreased with increasing the substrate temperature. The peak ratio of the h-BN aggregation is approximately equal

(a)   (b)

100 μm   5 μm
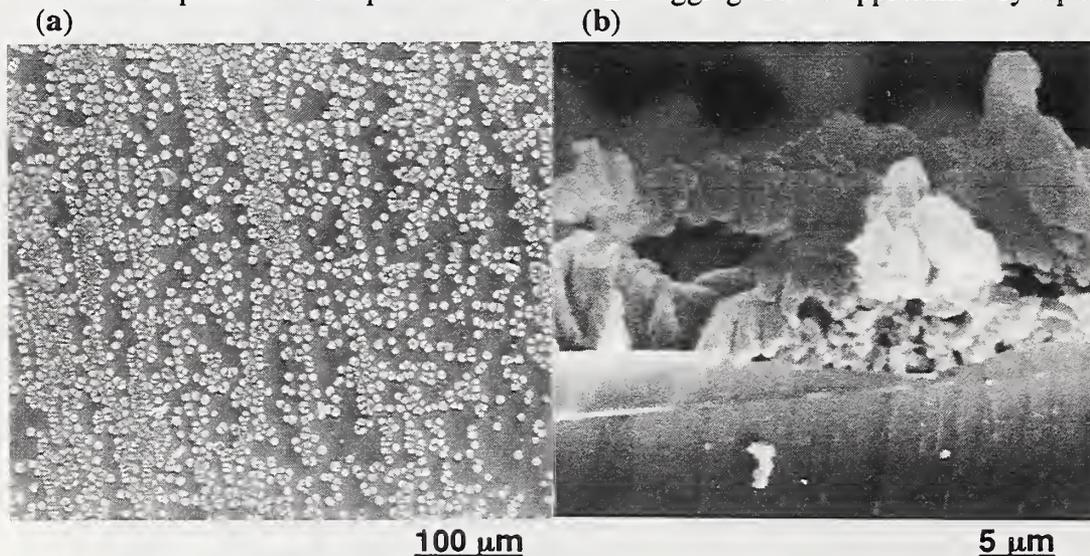
FIG. 1. SEM micrographs of the deposits synthesized at a substrate temperature of 400°C and negative bias of 450 V. (a) Top view and (b) cross-sectional image.

to that of standard *h*-BN sample, suggesting that the continuos films possess boron rich composition. There was no crystalline particle in the TEM image of the continuos boron nitride film deposited at a substrate temperature of 400°C and bias voltage of 450 V. Furthermore, in the high resolution image the grainy appearance in the image under optimum focusing conditions reveals that the continuos film is composed of noncrystalline or amorphous phase. These results are supported by the diffraction pattern which indicates only halo-rings. In the summary of the analytical works, deposits we obtained here are boron nitride having two phases, *i.e.*, *h*-BN aggregation and amorphous boron nitride film.
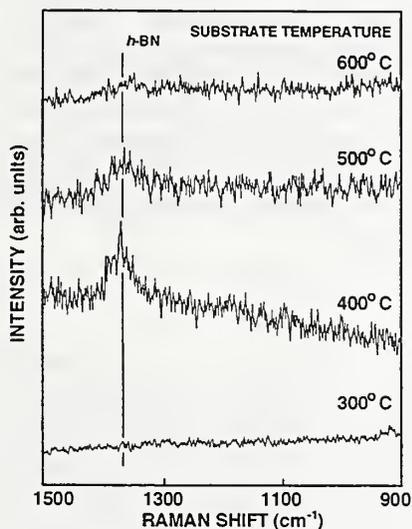
FIG. 2. Raman spectra obtained from dendritic aggregation on the sample.
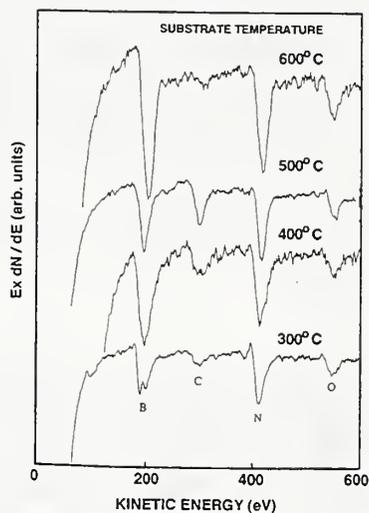
FIG. 3. Auger electron spectra of the samples. C and O peak were from the surface contamination.
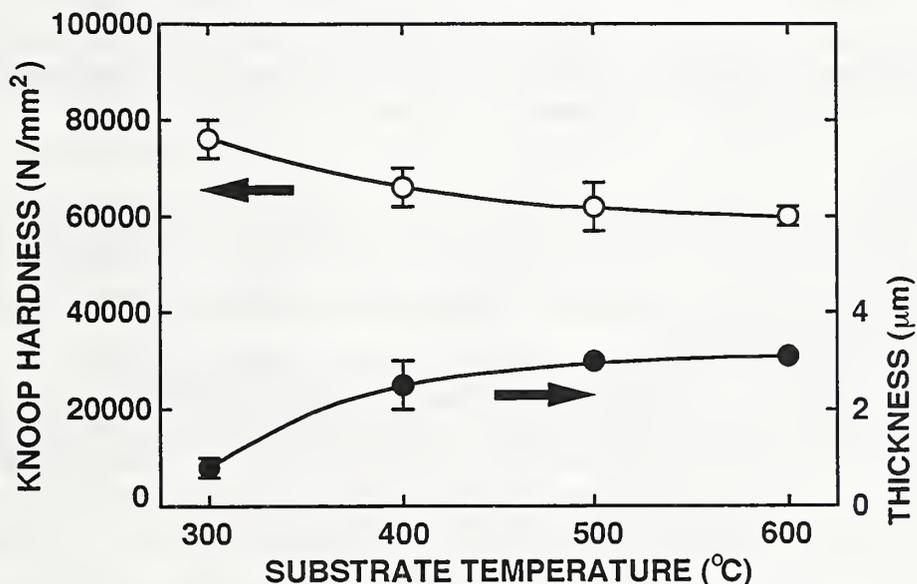
FIG. 4. Knoop microhardness and film thickness of the boron nitride films deposited at various substrate temperature.

Although h-BN aggregation was mechanically soft, amorphous boron nitride films showed Knoop hardness ranging 60000-80000 N/mm^2 to be comparable to that for bulk c-BN prepared by high pressure and high temperature techniques. However we have to note that hardness rapidly decreases with displacement on the depth profile of hardness. Figure 4 shows hardness changing with the substrate temperature during deposition. A total of five to ten indents were averaged to determine the mean hardness. Prior to measurement, force-hardness curves for the boron nitride films were obtained using loading force ranging 20 mN to 250 mN. Since the samples appeared microcrack at the condition of >100 mN, we maintained a maximum load of 100 mN for hardness measurements.

The surface of boron nitride films is completely unchanged by the attempt of scratch test using a diamond head, having 0.2 mm in diameter, with a maximum load of 20 N, suggesting good adhesion without any efforts to make the adhesive interlayer. With this condition, the critical load of diamond like carbon films prepared by the electron cyclotron resonance plasma enhanced chemical vapor deposition technique on the Si substrate was in range 16-18 N. These results present the very real possibility of the steady state growth of hard boron nitride films on several kinds of material with good adhesion by the plasma CVD techniques in the future.

4. Conclusion

Boron nitride samples were synthesized using plasma CVD apparatus with BCl_3-N_2-H_2-Ar. Deposits on the Si substrate were boron nitride having two phases, $i.e.$, h-BN aggregation and amorphous boron nitride film. The surface of the amorphous boron nitride films indicated a Knoop hardness of 60000-80000 N/mm^2 at a loading force of 100 mN. Scratching test revealed that the critical load of the boron nitride films are higher than that of diamond like carbon films prepared by the electron cyclotron resonance plasma enhanced chemical vapor deposition technique.

Acknowledgment

References

1. A. Chayahara, H. Yokoyama, T. Imura and Y. Osaka, Jpn. J. Appl. Phys. **26** (1986) L1435.
2. H. Saitoh, T. Hirose, H. Matsui, Y. Hirotsu and Y. Ichinose, Surf. Coatings Technol. **39/40** (1989) 265.
3. H. Saitoh and W. A. Yarbrough, Appl. Phys. Lett., **58** (1991) 2228.
4. H. Saitoh and W. A. Yarbrough, Appl. Phys. Lett., **58** (1991) 2484.
5. H. Saitoh and H. Morino and Y. Ichinose, Jpn. J. Appl. Phys. **32** (1993) L1684.
6. H. Saitoh, T. Hirose, T. Ohtsuka, and Y. Ichinose, Appl. Phys. Lett. **64** (1994) 1638.
7. R. Geick and C. H. Perry, Phys. Rev. **146** (1966) 543.

Mechanical properties of nitrogen containing carbon films prepared by ECR plasma CVD

Tohru Inoue, Shigeki Tsubata, Shigeo Ohshio, Hidetoshi Saitoh, and Kiichiro Kamata

Department of Chemistry, Nagaoka University of Technology,
Kamitomioka, Nagaoka, Niigata 940-21, Japan.

Key words; C:N films, DLC, ECR plasma, CVD, Knoop hardness, scratching test

Abstract

ECR plasma CVD apparatus was employed to deposit nitrogen containing carbon (C:N) films. In this apparatus, negative dc bias voltage was applied to the substrate for acceleration of the positive ions toward the substrate. The deposition conditions are effective to change the mechanical properties of the films. Knoop micro hardness measurement and scratching test were performed to compare mechanical properties between C:N film and diamond-like carbon film.

1. Introduction

There have been increasing efforts to synthesize the hypothetical compound β-C_3N_4 [1,2], with C substituted for Si on the β-Si_3N_4 at its crystalline form, by several methods including the phase transition techniques and the vapor deposition methods [3-8]. We have synthesized hard diamond-like carbon (DLC) films using an ECR plasma CVD apparatus [9]. In this, ion acceleration by applying bias voltage between plasma and substrate is significantly effective in producing sp^3 hybridized C-C bond in the films [10], implying that the ions possess relatively high kinetic energy for changing bonding status. This provides a motivation to use ECR plasma CVD system to form β-C_3N_4 or related materials. We propose that high energy bombardment of carbon and nitrogen ions toward the surface of the substrate is effective to introduce nitrogen to the growing films, and thus to vary the mechanical properties.

2. Experimental procedure

The C:N and DLC films were prepared by an ECR plasma CVD apparatus (Tokki Co. ECV-250) [9]. The preparation conditions of the films are followed as shown in Table 1. Knoop hardness (Hk) of C:N films was determined using the micro hardness tester with a rhombic Knoop indentor at a loading force of 10 gf for 20 seconds. Using the scratch-tester with a diamond coan having a radius of 0.2 mm, the critical load (Lc) and the frictional coefficient (Fc) of the C:N films on Si(100) substrate was determined. The scratch-test was performed under these conditions; a maximum load of 23 N with a increasing rate of 23 N/min during the scanning length of 5 mm.

Table I Preparation conditions

CH_4 gas flow rate	30 cm³/min
H_2 gas flow rate	30 cm³/min
N_2 gas flow rate	0-40 cm³/min
Total gas pressuer	3.2×10^{-1} Pa (DLC)
	8.0×10^{-2} Pa (C:N)
Microwave power	200 W
Magnetic flux density	0.0875 T
Bias voltage	0-400 V (negative)
Substrate temperature	200 °C
Substrate	Si (100)

3. Results and discussion

At the condition of $[N_2]/([CH_4]+[N_2])$ gas flow rate ratio of 0.5, the effects of dc bias voltage and total gas pressure on the growth rate of resulting films are shown in Fig.1. At 3.2×10^{-1} Pa deposition, there is a typical local maximum of the growth rate at about 50 V. At the range of $\geq$ 50 V, the growth rate of the films decreased with increasing negative dc bias voltage, and finally no film was deposited over 100 V. At relatively high bias conditions, the result of one-dimensional surface step measurement indicated that the height of the surface of the substrate was lower than that of the part masked before deposition, implying the surface etching of the substrate through ion bombardment.
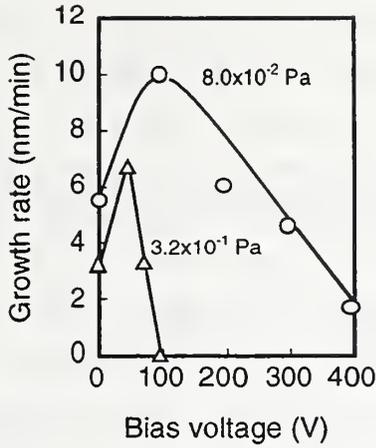
Fig.1 Relationship between bias voltage
and growth rate of C:N films
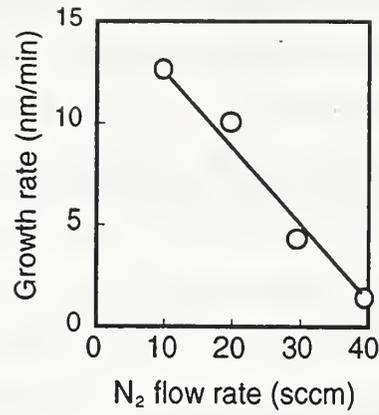
Fig.2 Relationship between N2 gas flow
rate and growth rate of C:N films

In this process, both hydrocarbon ions and nitrogen ion should have important role for both deposition and etching of the films. Our previous report indicated that the growth rate of the carbon films showed a monotonically increasing with negative bias voltage up to 200 V, at the condition without nitrogen.[9] This implies that bombardment of hydrocarbon ions may not contribute as much as nitrogen to sputter the growth film. As shown in Fig. 2, with increasing the $[N_2]/([CH_4]+[N_2])$ gas flow rate ratio in a constant CH_4 and H_2 gas flow rate of 30 cm^3/min each, the growth rate of the films decreased. This reduction of growth rate also suggest that bombardment by nitrogen ions is more dominant for etching of growing films than hydrocarbon ions.
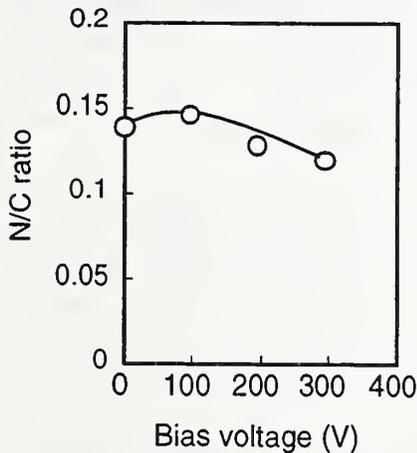
Fig.3 Relationship between bias voltage
and N/C ratio of C:N films
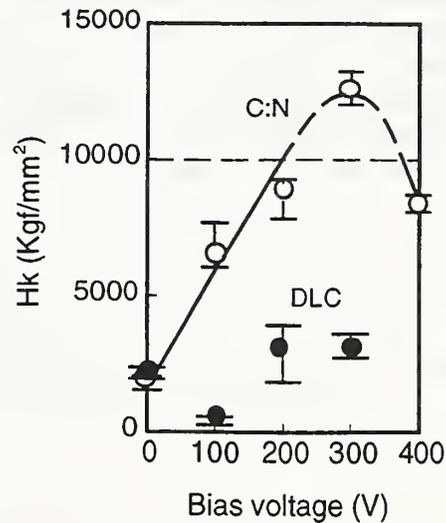
Fig.4 Relationship between bias voltage
and Knoop hardness of C:N films

The effect of negative dc bias voltage on the nitrogen content in the film was evaluated with the intensity ratio of the N(KLL) to C(KLL) peaks in the spectra. Figure 3 indicates that the N(KLL)/C(KLL) intensity ratio slightly changed between 1.25-1.5 with bias voltage. Knoop hardness at the surface region of the films was varied with bias voltage as shown in Fig.4. This results suggest that Knoop hardness is higher than that of DLC films. However we have to note that hardness rapidly decreased with displacement from the surface on depth profile of hardness. On the other hand, frictional coefficient (Fc) of DLC and C:N films determined by the scratch-test apparatus mainly decreased with the dc bias voltage. In addition, it was found that Fc of C:N films lower than that of DLC films.

Acknowledgment

References

[1] A.Y.Liu and M.L.Cohen, Science **245**, 841 (1989).
[2] A.Y.Liu and M.L.Cohen, Phys.Rev.B **41**, 10727 (1990).
[3] T.Sekine, H.Kanda, Y.Bando, and M.Yokoyama, J.Mat.Sci.Lett. **9**, 1376 (1990).
[4] M.R.Wixom, J.Am.Ceram.Soc. **73**, 1973 (1990).
[5] D.Li, Y.H.Chung, M.S.Wong, and W.D.Sproul, J.Appl.Phys. **74**, 219 (1993).
[6] N.Nakayama, Y.Tsuchiya, S.Tamada, K.Kosuge, S.Nagata, K.Takahiro, and S.Yamaguch, Jpn.J.Appl.Phys. **32**, L1465 (1993).
[7] C.Niu, Y.Z.Lu and C.M.Lieber, Science **261**, 334 (1993).
[8] D.Marton, K.J.Boyd, A.H.Al-Bayati, S.S.Todorov, and J.W.Rabalais, Phys.Rev.Lett. **73**, 118 (1994).
[9] K.Kamata, T.Inoue, K.Maruyama, and I.Tanabe, Jpn.J.Appl.Phys. **29**, L1203 (1990).
[10] P.Couderc and Y.Catherine, Thin Solid Films **146**, 93 (1987).
[11] C.C.Chang, Surface Sci. **25**, 53 (1971).
[12] R.N.Yasko and R.D.Whitmoyer, J.Vac.Sci.Technol. **8**, 733 (1971).

Ultradispersed diamond powders of detonation nature for polishing X-ray mirrors

N.I. Chkhalo [1], M.V. Fedorchenko [1], E.P. Kruglyakov [1], A.I. Volokhov [1],
K.S. Baraboshkin [2], V.F. Komarov [2], S.I. Kostyukov [2], E.A. Petrov [2]

[1]*Budker Institute of Nuclear Physics, Siberian Branch of the Russian Academy of
Sciences, 630090 Novosibirsk, Russian Federation*
[2]*NPO Altai, 659322 Biysk, Russian Federation*

Key words: ultradispersed diamond, polishing, roughness.

Abstract

The first experiments on the use of ultradispersed diamond powders of detonation nature for finish polish of X-ray optical elements are reported. The roughness values presently achieved for a number of materials are given.

l. Introduction

The short wavelength of X-rays requires a high quality of the surface of the optical elements, as estimations show that the admissible magnitude of roughness for grazing an incidence optics is 1.0 nm. For normal incidence optics (multilayer-based optics), the roughness required is a few angstroms or smaller. The surface roughness is determined by the size of abrasive material mains. The polishing materials used in the national industry such as krokus, polirit, diamond micropowders of static nature and some others have grain sizes exceeding 0.1 μm.

In the present work it is proposed to use ultradispersed diamond powders of detonation nature (UDD) for finish polishing the elements of X-ray optics. The basic physicochemical properties of UDD are briefly described. Also presented are the data on roughness values obtained after polishing melted quartz, optical glass, nickel electro-chemically deposited on the copper substrate and sapphire coating obtained by means of a microplasma oxidizing method on an aluminum substrate [1].

2. UDD synthesis and their properties

Detonation synthesis of ultradispersed diamond powders differs from the other known ways of artificial diamond production in the following: The synthesis is realized in a

detonation zone due to coagulation of carbon atoms from the molecules of explosive materials [2]. The diamond particles obtained are a few nanometers in size and are distinguished by high reproduction of the sizes from operation to operation. The particles contain up to **50%** of the non-diamond phase of carbon. The product obtained is purified chemically from the non-diamond phase. The powders obtained in this way contain particles which practically have no sharp angles and are aggregated into clusters. The average size of the particles obtained by the method of small angle X-ray scattering is 5.0 nm. The air-dried product is agglomerated into granules which are able to partially dissociate into smaller particles upon ultrasonic dispersion in liquid media. More information on the physico-chemical properties of UDD is given in Ref.[3].

3. Experimental results

Substrate grinding and polishing were carried out on standard equipment by a deep-polishing method which is characterized by the fact that at every stage of treatment the thickness of the removed material is two times larger than that of the abrasive particles used at the previous stage. Silicon carbide, polirit, and UDD containing suspensions were used for grinding, polishing, and superpolishing, respectively. The main parameters of polishing process are: polisher material is tin, fixing pressure of polished material is 12 N/m^2, polisher rotational speed is 3600 sec^{-1}.

The surface roughness was measured by a method based on the angular dependences of the reflection coefficients $R_m(\vartheta)$ at a radiation wavelength $\lambda = 0.154$ nm from a tested substrate [1]. The influence of the roughness σ on the dependence $R_m(\vartheta)$ is incorporated by the formula

$$R_m(\vartheta) = R_i(\vartheta)\exp\left(-(4\pi\sigma\sin(\vartheta)/\lambda)^2\right),$$

where $R_i(\vartheta)$; is the reflection coefficient from an ideal surface, and ϑ is the grazing angle.

Fig. 1 presents the dependences $R_m(\vartheta)$ for a sample of melted quartz: the squares are for the experimental curve obtained after polishing with polirit, the crosses are for polishing with an UDD containing suspension, and the solid lines are theoretical curves corresponding to different roughness values. One can see that using suspensions with UDD enhances the roughness from 1.0 nm to 0.25-0.3 nm.

Similar dependences for nickel electro-chemically deposited on a copper substrate are given in Fig. 2. As is clearly seen from this figure, the best agreement between experiment and theory is observed at a roughness of 1.0 nm. The data on the achieved values of roughness and the values variation when using suspensions with different degrees of purification are presented in Table I.
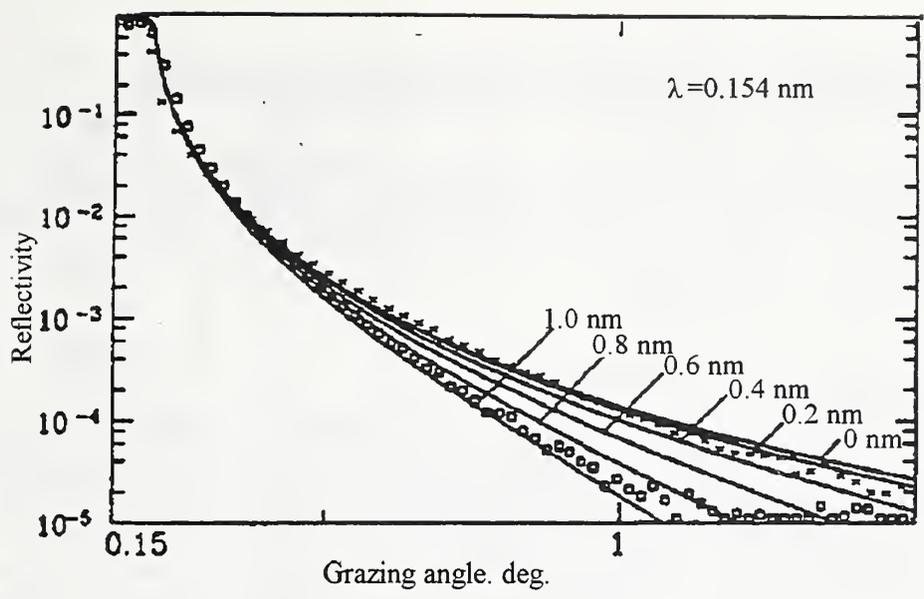
Fig. 1. Rocking curves for a sample of melted quartz: the squares indicate the experimental curve obtained after polishing with polirit, the crosses correspond to polishing with a UDD containing suspension, and the solid lines are for the theoretical curves corresponding to different roughness values.
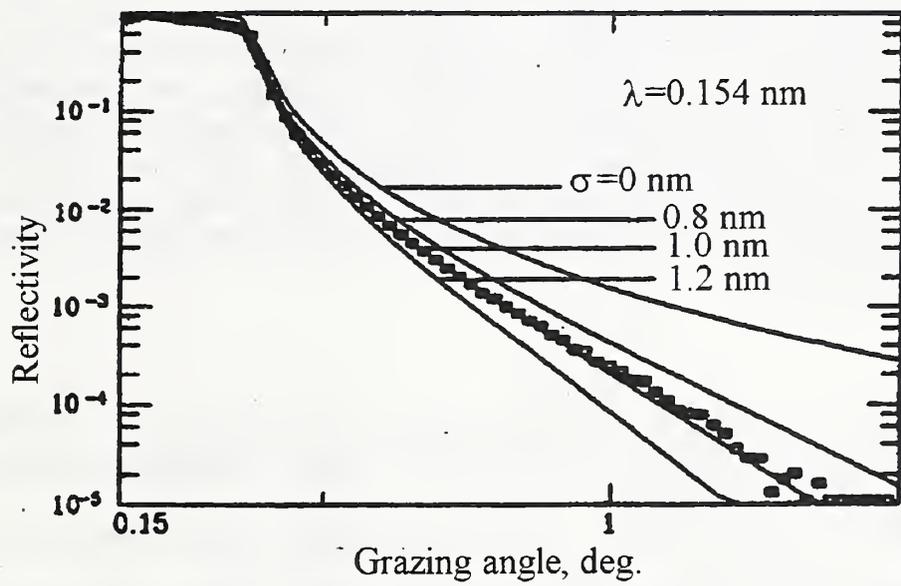
Fig. 2. Rocking curves for a sample of nickel electro-chemically deposited on a copper substrate: the squares indicate the experimental curve obtained after polishing with a UDD containing suspension, and the solid lines are for the theoretical curves at different roughness values.

Table 1
Roughness values obtained with polishing by UDD containing suspensions

Substrate material	Best roughness [nm]	Roughness Variations [nm]
Melted quartz		
Glass **K8**	0.3	0.3-0.9
Electro-chemically deposited nickel	0.5	0.5-1.0
Silicon	1.0	1.0-1.2
Sapphire obtained by microplasma oxidizing of	0.6	0.6-1.0
aluminum substrate	1.7	1.7-2.0

The advantages of the UDD containing suspensions manifest themselves when polishing silicon. For obtaining a surface roughness of silicon at an angstrom level chemical – mechanical or chemical-dynamical polishes are used as a rule. However, because of the very high rate of etching, it is practically impossible to obtain a good geometry of the surface. Polishing with UDD containing suspensions proceeds at the same rates as for quartz and provides a much better surface geometry.

4. Conclusion

A new polishing material – ultradispersed diamond powders of detonation nature with an extremely small size of initial particles (average size: 5.0 nm) – was used for the first time. Using this material for polishing X-ray optical elements from melted quartz, optical glass, silicon and electro-chemically deposited nickel gives us very good results. Therefore we consider this material as a very promising composite of polishing suspensions. The latter can be applied not only to superfine polish of X-ray optics, but also to treatment of optical materials and crystals (NaC1, KC1, rubies, sapphires, etc.) for ultraviolet, visible and infrared optics, in engineering and other industries, where abrasive materials are used.

References

[1] I.A. Bushuev, V.A. Chernov, N.I. Chkhalo, M.V. Fedorchenko, V.I. Kirillov, A.V. Lunegov and A.A. Nikiforov, Proc. 4th Int. Conf. on X-Ray Microscopy, Chernogolovka, 1993, H-11, in press.
[2] A.I.Lyamkin, A.P. Ershov, E.A. Petrov et al., DAN 302 (3) (1988) 611, in Russian.
[3] A.L. Vereshagin, G.V. Sakovich, V.F. Komarov and E.A. Petrov, Diamond and Related Materials 3 (1992) 160.

ERRATUM

In the article, **In-Situ Temperature Measurement on Diamond-Coated Tools: A New Instrument for Optimizing Cutting Processes** by P. Müller-Hummel and M. Lahres which appears on page 191 of the Proceedings, the **Acknowledgement** section is modified as follows:

Acknowledgements

The authors thank Mr. W. Fabian, Mr. K. Griesinger and Mr. W. Luik for parts of experimental work and Mr. X. Liu for help in drafting this article.

ERRATUM

In the article, **High Temperature Diamond Film Deposition on a Natural Diamond Anvil** by T.S. McCauley and Y.K. Vohra, which appears on page 377 of the Proceedings, the **Conclusions** section is modified as follows:

4. Conclusions

In conclusion, we report for the first time the deposition of a high quality diamond layer on a type Ia natural diamond anvil by MPCVD at a substrate temperature between 1800°-2100° C. The growth rate for this process is estimated to be between 50 and 400 µm/hr. We believe that the presence of large concentrations of C_2 are critical to the observed rapid growth. Raman analysis confirms the crystallinity and phase purity of the deposit. Low temperature PL measurements show the enhanced incorporation of optical defect centers with ZPLs at 636, 575 nm due to the unintentional incorporation of nitrogen [1], and 737 nm due to silicon [6] (perhaps from the quartz microwave window). PL excitation studies of the 775 nm band, the origin of which is unknown [4], reveal that it is selectively pumped in the green ($\sim$ 500 nm) spectral region. Further investigation of this explosive diamond growth regime at high temperature is in progress, as is the development of further optical and direct methods to measure substrate temperature in-situ.

THEORETICAL STUDY OF EXTENDED LATTICE DEFECTS IN DIAMONDS

Kinichi Masuda-Jindo

Department of Materials Science and Engineering, Tokyo Institute of
Technology, Nagatsuta, Midori-ku, Yokohama 227, Japan

Abstract

The atomistic configurations and electronic states of extended lattice
defects (dislocations and grain boundaries) in diamond crystals are
investigated in conjunction with their mechanical properties by using the
tight-binding (TB) recursion electronic theory. It is shown that the atomic
configurations and electronic states of mobile dislocations (30° and 90°
partial of $1/2<110>$ {111 } lattice dislocation) are similar in nature to
those of Si crystals. However, it has been found that the cleavage strength
of the grain boundaries in diamond is only slightly reduced ($\sim 10\%$) with
respect to those of the single crystals; the amount of the reduction is
considerably smaller than that of Si crystals.

1. Introduction

Diamond is very interesting material both from fundamental and technological
points of view. In Table I (left column), we summarize the fundamental
properties of diamond crystals. Diamond is unstable with respect to
graphite, but the difference in free energy between diamond and graphite is
very small, 2.900 kJ/mol (~ 0.03eV/atom) at 298K and 1 atm pressure.
Furthermore, there is a very large activation barrier inhibiting the
transformation of diamond to graphite. Therefore, nucleation of diamond
occurs through graphitic intermediates or by growth on diamond debris left
from scratching [1]. The morphologies of vapour-grown (CVD) diamond
crystals include: spherical clusters of diamond microcrystals, cubes, cubo-
octahedrons, octahedrons and flat hexagonal platelets: Complex, multiply
twinned forms (e.g., decahedrons and icosahedrons) are observed. It has
also been observed that stacking errors (faults) formed during growth
enhance growth rates and strongly influence the final crystal morphology.
In CVD diamond films, competitive growth between adjacent grains develops a
cone-like columnar grain structure perpendicular to the substrate.
Dislocations within each grain fan out as the grains grow in cross sectional
area so that the dislocation density N_d decreases as the inverse square of
the distance Z from the substrate side of the film [1].

Dislocations in diamond are important in discussing electrical, mechanical
and thermal properties of diamonds: They act as electrically active defects

and can be ''structural dopants" (acceptors and/or donors), recombination centers reducing the lifetime of minority carriers, or scattering centers [2]. Phonons can be scattered by dislocations and this scattering significantly influences the thermal conductivity of the diamonds. Most dislocations in diamonds lie parallel to the crystal growth direction. Dislocations parallel to the direction of phonon motion scatter phonons strongly. Consequently, the thermal conductivity of CVD films parallel to the surface is less than the thermal conductivity perpendicular to the surface. Point defects (impurities) in diamond also provide us interesting phenomena. For instance, it is known that only boron, nitrogen and hydrogen dissolve in diamond. Hydrogen occupies a substitutional site in CVD diamond where it forms a sp^3 covalent bond with a neighbouring carbon atom. Substitutional hydrogen thus will scatter phonons and decrease the thermal conductivity as has been observed [1].

In order to understand the above mentioned experimental observations, it is highly desirable to perform theoretical calculations on the atomistic structures and fundamental properties of the lattice defects in diamonds. It is the purpose of the present study to investigate the atomistic and electronic structures of extended lattice defects (dislocations and grain boundaries) in diamond crystals by using the TB recursion electronic theory. We will discuss the physical (mechanical) properties of diamonds in terms of the calculated electronic and atomistic structures.

Table I. Physical properties (left) and TB parameters (eV) of diamond.

lattice constant	3.568 Å	E_s	-4.545
hardness	10 mg mm^{-2}	E_p	3.84
Young's modulus	945 GN m^{-2}	E_s *	11.37
thermal condutivity	20 W cm^{-1}K^{-1}	ssσ	-5.681
refractive index	2.42	spσ	6.591
band gap	5.45 eV	ppσ	6.795
density	3.51 g cm^{-3}	ppπ	-1.958
		spσ *	3.555

2. Principle of Calculations

To calculate the atomic configurations of the dislocations and grain boundaries in diamond, we use the transferable TB scheme[3] and the quenched molecular dynamics method[4]. We assume that the total energy of the system can be given by a sum of the band structure energy E_b and the pairwise repulsive energy E_{rep} contributions: $E_{tot} = E_{bs} + E_{rep}$. The electronic eigenvalues are obtained by solving an empirical TB Hamiltonian H_{TB}. The off-diagonal elements of H_{TB} are described by a set of orthogonal sp^3 two-center hopping parameters, ssσ, spσ, ppσ and ppπ (-5.0, 4.7, 5.5, and -1.55 eV, respectively), scaled with interatomic separation r as a function of s(r) [3]; and the on-site elements are the atomic orbital energies of the corresponding atom (E_s = -2.99 eV, and E_p = 3.71 eV). The remainder of E_{tot} is modelled by a short-ranged repulsive term E_{rep} given by $E_{rep} = \Sigma f \{ \Sigma \phi (r_{ij}) \}$, where $\phi (r_{ij})$is a pairwise potential between atoms i and j, and f is a functional expressed as a 4th-order polynomial

with argument $\Sigma_j \phi(r_{ij})$ [3]. It has been shown that this type of
transferable TB scheme reproduce excellently the total energy curves of the
two most stable structures, graphite and diamond, in good agreement with
the results of LDA (local density approximation) calculations.

To calculate the detailed electronic structures around the extended lattice
defects, we use the TB recursion formalism based on sp^3s^* basis orbitals
[5]: The TB parameters of this model are presented in Table 1 (right column)
. This model reproduces the principal features of the elemental and compound
semiconductor conduction band structures, particularly near the Γ and X
points of the Brillouin zone. The atomic energy levels E_s , E_p and E_s^*
are shifted rigidly so as to ensure the local charge neutrality in the
crystal containing the extended lattice defects. The recursion coefficients
are calculated up to 34th level for the clusters of about 38400 atoms.

3. Results and Discussions

Using the LCAO recursion method of sp^3s^* basis orbitals, we have calculated
the atomic configurations and electronic states of dislocations, 30 ° and 90
° partials of 1/2<110> {111 } dislocation, in diamond crystals. Particular
attention has been paid on the determination of gap states associated with
the straight dislocation line as well as the point-like singularities like
''soliton" or kink-site atoms. In Fig.1, we present, by solid curve (dashed
curve: perfect crystal), the calculated local electronic DOS on the soliton-
site atom (marked by▲ in the figure 2a) in the core of 90° partial
dislocation in diamond. In these calculations, it is interesting that the
prominent deep levels of ''solitons" (located near the center of the band
gap) appear even for the reconstructed core with small atomic displacements.
No prominent deep levels have been found for atomic sites in the
reconstructed cores and at the kink-site atoms. The reason for the absence
of the gap states in the kink-site atom is due to the fact that the kink-
site atom (with three nearest-neighbours with one missed bond) has a
strongly compressed bond, and it compensates the effect of the missed bond.
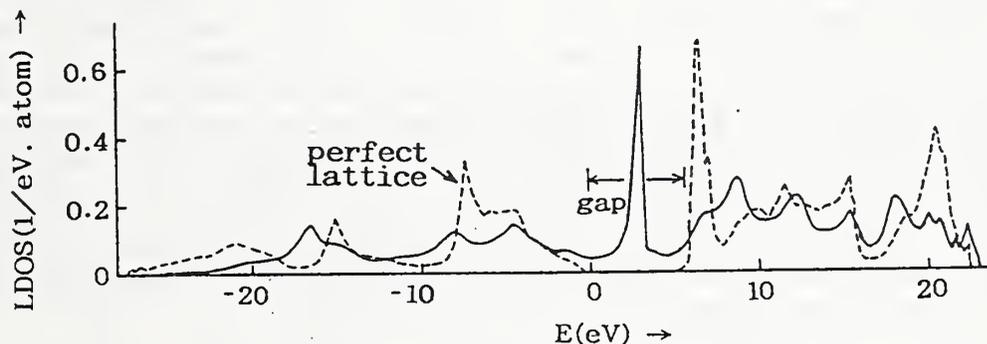These characteristics are similar in nature to those of Si crystals.

Fig.1 Local DOS on soliton site atom in the core of 90° partial in diamond.

We now discuss the strength properties of CVD diamond crystals in
conjunction with the fracture morphorgy, i.e., intergranular or
transgranular mode. We have chosen Σ =3 and Σ =9 [110] symmetrical tilt
grain boundaries in diamond crystals and calculated the atomic

configuration and local electronic structures. Figure 2(b) shows the calculated atomic configurations in the (stable) core of the $\Sigma=9$ tilt grain boundary in diamond. There are two kinds of atomic configurations for $\Sigma=9$ tilt grain boundary in diamond cubic crystals. The type A has a glide-plane symmetry with a sequence of 5- and 7-membered rings (very reminiscent of the Si(111) 2x1 surface reconstruction). On the other hand, the type B has a mirror symmetry with a linear sequence of 7-, 6- and 5-membered rings. We have found that the grain boundary with type A structure is more stable than that with type B structure, as in Si or Ge crystals.
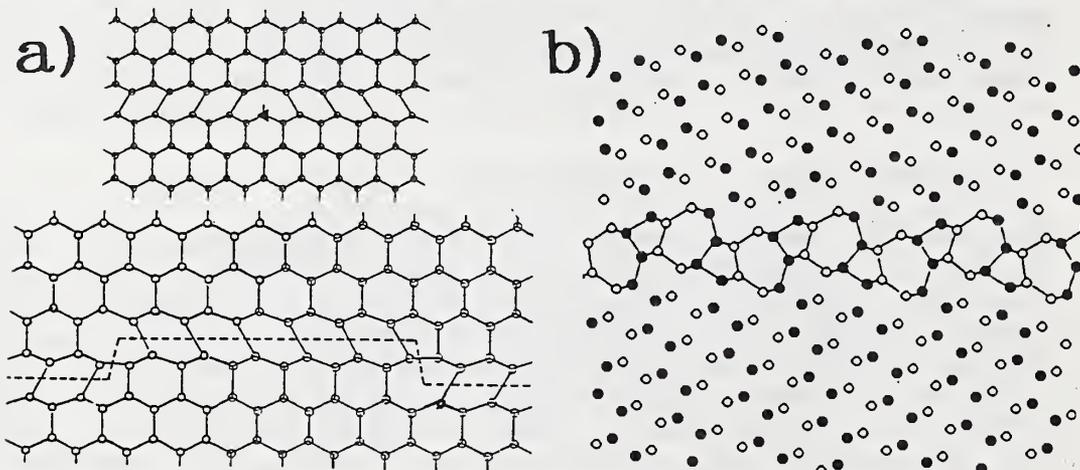

Fig.2 The atomic configurations of 90 ° partial dislocation with kinks and soliton (a), and $\Sigma=9$ {122 } tilt grain boundary in diamond (b).

The cleavage strength of the grain boundary is calculated as follows: The two halves of the diamond crystal with surface index (l,m,n) are separated rigidly in the <l,m,n> direction, with no surface relaxation and no reconstruction. The cleavage test of this type is based on the fact that for covalent semiconductors like diamond, the energy reduction due to the surface relaxation or reconstruction is generally small ($\sim$a few percent) compared to the surface energy, and not of primarily importance. The calculated cleavage strength f_{gb}/f_{sc}, divided by that of the single crystal, are 0.951 and 0.902 for $\Sigma=3$ and $\Sigma=9$ tilt grain boundaries in diamond, respectively. These values are relatively larger than those of Si crystals. This tendency on the grain boundary strength can be favourably compared with the experimental observation on diamond crystals [1]. For instance, there have been many examples of transgranular fracture from scanning electron microscopy observation of the fracture surfaces of the eroded films. Transgranular fracture is also common when free-standing films are broken by bending. These observations of transgranular fracture suggest that the grain boundaries in CVD diamond are strong enough.

4. References

[1] A.Lettington and J.W.Steeds, "Thin Film Diamond",(Chapman & Hall, 1994)
[2] H. Alexander and H. Teichler, Mater. Sci. and Tech. 4, (1991) 249.
[3] C.H.Xu,C.Z.Wang,C.T.Chan and K.M.Ho, J.Phys.Condens.Matter 4(1992)6047.
[4] K. Masuda-Jindo, Solid State Phenomema 37-38, (1994) 125-130.
[5] P.Vogl, H.P.Hjalmarson and J.D.Dow, J.Phys.Chem.Solids 44,(1983) 365.

Comparison of Diamond-like Carbon and Polycrystalline Diamond Films for High Temperature Capacitors.

P.B. Kosel[1], D. Wu[1], O.P. Kosel[1], S.F. Carr[2], A. Garscadden[2], P.R. Emmert[2], R.L.C. Wu[3]

[1]Department of Electrical and Computer Engineering, University of Cincinnati, Cincinnati, OH 45221
[2]Wright Laboratories, Wright-Patterson AFB, Dayton, Ohio 45433-6563
[3]K Systems Corporation, 1522 Marsetta Drive, Beavercreek, OH 45432

Abstract

Both diamond-like carbon and polycrystalline diamond films have been obtained with resistivities exceeding 10^{10} ohm-cm and dielectric constants of 4.0 and 5.8, respectively. These films are chemically inert and have great mechanical hardness, high melting points and high thermal conductivity. The combination of these properties suggests their use as capacitor dielectrics for monolithic circuits destined for high-voltage and high-temperature operation. Parallel plate capacitors formed with 0.5 μm diamond-like carbon films exhibit capacitances of 13 nF cm^{-2} and interdigitated capacitors fabricated on thick (>300 μm) polycrystalline diamond films provide typical capacitance values of around 100 pF cm^{-2}. The equivalent series resistances at low frequencies (10^2-10^3 Hz) of these capacitors in both cases have been found to be low making them potentially useful in filter circuit applications.

1. Applications

Capacitors are present in all electronic circuits and are usually the most vulnerable of the components present particularly when high voltages and high temperatures are involved. Thus capacitor reliability is a dominant issue in circuits used in power conversion and control systems in automobiles, aircraft and industrial machinery. Two basic forms of capacitors are generally used in monolithic circuits: the parallel-plate and the interdigitated-electrode type. The type chosen is usually dictated by the processing conditions involved in the production of the dielectric. For diamond-like carbon (DLC) and polycrystalline diamond (PCD) films different substrate temperatures are required during growth.

A low temperature (<250 °C) has been found to be sufficient for good quality DLC film deposition. This offers maximum process flexibility without major process alteration to integrated circuit fabrication. Moreover, non-refractory substrates such as glass and aluminum can be used for making discrete devices. DLC films are usually smooth and the growth rates are low which limits practical film thicknesses to

0.2 to 2.0 μm. For the growth of high-resistivity PCD films high substrate temperatures (>850 °C) are necessary which limits the choice of substrate to refractory materials such as silicon and some refractory metals. For integrated circuit applications the incorporation of PCD films needs careful attention in the determination of the fabrication procedure.

The capacitance of a parallel-plate device is given by the simple formula

$$C = \frac{\varepsilon A}{t} \qquad (1)$$

where ε is the dielectric permittivity, A is the area of the capacitor and t is the dielectric thickness. For an interdigitated-electrode (or MSM) structure the capacitance in picofarads is given by

$$C = L(\varepsilon_r + 1)[0.089(N - 3) + 0.099] \qquad pF \qquad (2)$$

where L is the overlap finger length in centimeters, ε_r is the dielectric constant and N is the number of fingers. For filter applications in low frequency power circuits the capacitor dielectric needs to have low loss. The standard measure of this loss is the equivalent series resistance (ESR) which has a dependence on the resistivity and dielectric constant as given by

$$ESR = \frac{\rho \varepsilon / C}{1 + \left(\omega \rho \varepsilon\right)^2} \qquad (3)$$

where ρ is the resistivity of the material, C is the capacitance, ε is the film permittivity, and ω is the angular frequency.

2. Capacitor fabrication

DLC Capacitors: DLC films were formed using a high-current hydrocarbon beam in a stainless steel UHV chamber at low pressures (about 0.1 mTorr). The beam diameter was 20 cm and the RF exitation was 13.56 MHz [1]. The source gas was a mixture of methane, argon and hydrogen. The ion beam energies used were in the range of 50 eV to 3000 eV and an *in situ* quadrupole mass spectrometer was used to monitor the ionic species. The DLC film compositions were found by Rutherford back-scattering (RBS) to show a mean C:H ratio of 1.7:1. The DLC films could be deposited directly on aluminum at high energies which allowed simple parallel-plate capacitor structures to be formed. First long metal stripes were deposited through a shadow mask followed by DLC film deposition. The capacitors were then finished off by depositing square electrodes through a second shadow mask over the metal stripes.

PCD Capacitors: High resistivity PCD films were grown on bare silicon in a high-pressure plasma excited with microwave energy [2]. The properties of the films

were found to depend on the growth conditions. Best results were obtained with a gas composition of 0.7% CH_4 in H_2 at a pressure of 40 Torr. At a power of 1.5 KW and a substrate temperature of 950 °C the growth rate was about 0.3 μm/hr. The PCD films used for parallel-plate structures were 4-7 μm thick and had a root-mean-square (RMS) surface roughness of 6 to 160 nm. The graphitic content of the PCD films was checked by Raman spectroscopy for the presence of the 1560 cm^{-1} spectral line. For the PCD films reported here no discernable peak at 1560 cm^{-1} was evident.

To form parallel-plate capacitors on PCD films the films were first made free-standing by removal of the silicon by plasma etching [3]. The free-standing film areas were 8x8 mm^2 . The parallel-plate capacitors were then formed by depositing circular metal electrodes through a shadow mask onto the smooth side of the films and providing a uniform coverage of metal over the rough side. These capacitors are called DOT capacitors.

Thick (>300 μm) PCD plates were obtained from a commercial source and were large enough (1 cm^2) to be handled discretely. These were used for the fabrication of monolithic MSM structures by photolithography. Since the electrodes in this type of capacitor are located on the same side of the substrate they were fabricated using a single level photolithographic step. Both large and small MSM devices were produced. The largest MSM device occupied an area of 2x2.5 mm^2.

3. Electrical characteristics

DLC Capacitors: The DLC films were amorphous with thicknesses in the range of 0.3-1.0 μm. It was found that high deposition energy was needed during growth to promote adhesion of the DLC films to aluminum electrodes. Therefore, rapid thermal sintering was used to increase the adhesion of the first level aluminum to the silicon. Representative data for several films is listed in Table I. These show good values for resistivity, dielectric constant and the projected ESR for a 1 μF capacitor at 1KHz. The best ESR values were obtained for DLC films on glass substrates.

Table I. Summary of DLC capacitor measurements

Sample	Thickness μm	Capacitance nF/cm^2	Resistivity Ω-cm	Dielectric constant	ESR for 1uF @ 1KHz
DLCC2	0.3	12.0	8.9×10^{10}	4.1	0.78
AlGL1	0.63	5.1	2.1×10^{10}	4.0	3.4
AlGL2	0.66	4.8	6.7×10^{8}	3.6	76.3
AlSi6	0.73	11.0	1.2×10^{9}	8.7	26.6
AlSi7	0.82	8.3	1.4×10^{9}	7.7	25.8

PCD Capacitors: Two electrode spacings were used for the MSM devices: 5 μm and 10 μm. A straight single-gap MSM capacitor with a 5 μm gap size was also used. The current-voltage curves for the MSM structures were symmetric about the origin and voltage biases exceeding 100 volts could be applied without breakdown. The

leakage currents of the MSM capacitors were comparable in magnitude to those of the DOT capacitors .

The current-voltage characteristic for a DOT capacitor had the Schottky-diode shape characteristic of two back-to-back Schottky contacts one of which is small (a DOT) while the other is large (the ground plane). From the slope of the forward characteristic the film resistivity was found to be 9×10^{10} Ω-cm. The capacitance values for several sizes of DOT capacitor were measured at 1 MHz with a Boonton capacitance meter. Typical values are shown in Table II. The calculated dielectric constant for the PCD films from these values was 5.8 which is close to the accepted value for single crystal diamond. The voltage dependence of the DOT capacitances was also checked for the bias range of -30 to +30 volts at normal and raised temperatures up to 200 °C. The results show no voltage dependence of the capacitance even at high temperatures.

Table II. DOT Capacitors on PCD substrates

DOT dia mm	Capacitance pF	Resistivity Ω-cm	Dielectric constant	ESR for 1uF @ 1KHz
1.5	13.9	9×10^{10}	6.2	0.51
2.5	35.6	9×10^{10}	5.7	0.56
3.5	85.8	9×10^{10}	5.7	0.59

4. Conclusion

Test capacitors were fabricated on DLC and PCD films and the electrical properties have been meausred. The PCD film capacitors have been found to be stable at high voltages and at temperatures up to 200 °C. For both the DLC and PCD cases the ESR's of the capacitors were small enough for use in low frequency circuits.

6. References

1. R.L.C. Wu, W. Lanter, K. Miyoshi, S.L. Heidger, P. Bletzinger, A. Garscadden, Proc. of the 1994 MRS Meeting, Symposium A: Beam Solid Interaction for Materials Synthesis and Characterization, in press (1995).
2. R.L.C. Wu, A.K. Rai, A. Garscadden, P. Kee, H.D. Desai, K. Miyoshi, J. Appl. Phys., vol. 72, no. 1, p. 110-116 (1992).
3. P.B. Kosel, J. Iyer, S.F. Carr, A. Garscadden, P.N. Barnes, R.L.C. Wu, SPIE Proc. on Diamond-Film Semiconductors, vol. 2151, p. 121 (1994).

ALTERNATIVE GROWTH MECHANISMS IN THE NATURAL DIAMONDS

Gafitullina D.S., Ashurov M.Kh., Oksengendler B.L.

Institute of Nuclear Physics, Ulugbek, Tashkent,702132,Uzbekistan

Abstract

On the base of autoradiography method including digital treatment it was investigated the impurity distribution in natural diamonds.It was established the alternation of zonal and fibruilar distribution of several impurities. This phenomenon treatment may be realized on the base of combaing of Cahn-Routburd-Shklowskii [5-7] growth theory with Prigogine'like synergetic idea. According to [5-7] the type of crystallization mechanisms depends on relation between crystallization moviting force and value of combaine parameter, depending of boundary wide .A lot of regimes of crystallization including the alternation of normal and tangential mechanisms are discussed.

1. Introduction.

Evidence of growth kinetics and debate genesis questions of natural diamond is avaible only by an inderect way with decoding the paragenetic information contained in crystals,in particular, impurity composition of inner part[1-2].

Side by side examination of microdefects inner morfology attract attention investigators [3]. Impurity composition of inside part and topography of impurity distribution will can give new information adout growth mechanisms and.genesis of diamond. Crystal growth is unequal process. Growth mechanism of crystal, impurity concentration and distribution between different phases are depending on metastable level. Therefore impurity distribution can be the indikator of unequal conditions level though cannot solve: is impurity modificator of growth process? Among diamonds there are cubic crystals with fibruilar inner structure and define microdefects. Growth mechanisms are very debate of these objects.Using nuclear methods including digital treatment makes a new opinion about their genesis.

2.Experimental equipment.

The impurity distribution in diamonds was determined by autoradiography methods which make it possible to identify and quantitatively evaluate the impurities and define their distribution in the crystal bulk [1]. It is based on the secondary beta-irradiation registration. Analysis of autoradiographic features is connected with the elucidation of the optical density distribution of exposed and treated photoemulsion, used as a detector of the secondary beta-irradiation. Autoradiography treatment was conducted with the help of the dialoge system of the picture treatment, having matrix in 512x512 elements. The system allows to get 256 gradations of the grey colour. For vizualization of autoradiography the clastering analysis methodology in the tasks of the pattern recognition was used widely [4]. Impurities were identified by energy lines of the gamma spectra obtained and by half-life periods. The impurities content in a sample was evaluated by a relative method based on comparision of the radionuclidy activity of the element to identify with that of the reference.Gamma spectra of irradiated samples were measured by means of a Ge(Li)-detector and a multi-channel pulse analyses. For experimental purposes we selected twelve crystals of cubic habitus with grey colour.The selected crystals were used to cut <111> lamellae,then the latter were polished, chemically treated and exposed to the neutron flow of a reactor.

3.Results.

It was established three groups of impurity distributions among twelve cubic crystal. For first crystals it were found middle zone with very high concentration Mn,Co,Cu, Ni et.al., impoverished layer arround middle zone. By means of the vizualization of autoradiograms it was found little fibruilars in the middle region. For second crystals autoradiograms showed a fibriular impurity distribution for measures of weight of samples. Middle region was maked of scanty of impurities. For third crystals it was established: a) crosslike distribution,which was reflected diferrent absorption of octahedral and cubic
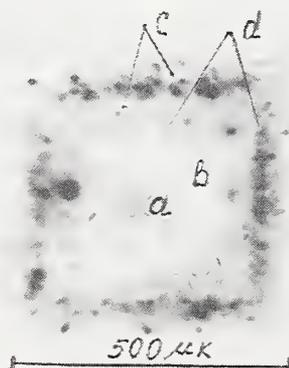

Fig.1. Impiruty distribution autoradiogram in cubic diamond:
a) middle zone Co-eriched,
b) sectorial distribution,
c) lammellar,
d) fibriular.

growth pyramids; b) little middle zone was riched of Co; c) for measures of weight it were alternative layers with impoverished of impurities and enriched of impurities with fibruilar distribution (fig.1). Thus for crystals with fibruilar structure it were found sectorial distribution, as well as alternation of lammellar and fibruilar impurity distributions.

4. Model.

The resalts obtained may be treated on the base of combaing of Cahn-Rourtburd-Shklowskii growth theory[5-7]. It has been considered boundary between of the crystal and melting going with the rate u along axis z. Let the creative energy for one atom in crystallization is Q ; T_o, T and T_f are temperaturies of equilibrium phase transition, environment and front crystallization correspondlly; χ and λ - temperature-conductivity and heat-conductivity of meduim. Then taking into account the nonlinear dependence u(T) [6], heat-exchange of medium one can write following form:

$$(1)\begin{cases} \dfrac{\partial T}{\partial t} = \chi \dfrac{\partial^2 T}{\partial x^2} + \dfrac{\chi}{\ell_{II}} \cdot \dfrac{\partial T}{\partial z} - \dfrac{\chi}{\ell_{\perp}^2} \cdot \left(T - T_0 \right) \\[3mm] QU = \lambda \left[\dfrac{\partial T_f^1}{\partial z} - \dfrac{\partial T_f^2}{\partial z} \right] \\[3mm] U = U_0 e^{-E/kT} \left[\exp\left(-Q/kT_0 \right) - \exp\left(-Q/kT \right) \right] \end{cases}$$

For boundary conditions $T\big|_{\pm\infty} = T_0$ and continious of temperature at the crystallization front lead to

$$(2)\begin{cases} T_1(z) = T_0 + \left(T_f^1 - T_0 \right) \exp\left(-\gamma_1, z \right) z > 0 \\[3mm] T_2(z) = T_0 + \left(T_f^2 - T_0 \right) \exp\left(+\gamma_2, z \right) z < 0 \end{cases}$$

- where $\gamma_{1,2} = \left[(1 + v^2)^{1/2} \pm 1 \right] / 2\ell_{II}; \ell_{II} = \chi/u; \ell_{\perp}^2 = \chi\tau_0$
- τ - characteristics of heat-exchange time, $v = \upsilon/u$,

T investigate the different regime of boundary moving incluced by rate fluctuation $\delta u_f = u_f - \dfrac{du}{dT}\delta T_f$ it is necessary to analys the signs of values [7].

$$(3)\begin{cases} D \equiv \mu^2 + 2B\mu + A \\ F \equiv \pm\frac{1}{4}\left(\mu - \sqrt{A}\right)^2 + \mu^2 + 2B\mu \end{cases}$$

where $\mu \approx Q/cT$; $A = 1 + v^2/u^2$; $B = \left(v^2/u^2 - 3\right)\sqrt{1 + v^2/u^2}$

c - heat-capasity of medium.

According to different signs of D and F it may be realized different crystallization regimes: homogenical, bistable, oscillating. So, if there are D< 0 and F>0, it may be realized stable oscillating regime of crystalization process. The stable oscillating regime needs of following conditions:

1)the small speed of heat-exchange (v<u),

2) the metastablity of initial state must be limites in special range:

$\frac{Q}{c}\xi_1 < T_0 - T < \frac{Q}{c}\xi_2$, where ξ_1 and ξ_2 are the function deducing from (3).

5. Discussion.

The results obtained show that in the growth process impurity distribution was put periodical transitions: lammellar $\rightarrow$ fibruilar $\rightarrow$ lammellar $\rightarrow$ fubruilar... Since the description impurity distribution is due to growth conditions deviation from the thermodynamic equilibrium at the crystallization front, periodical transition impurity distribution helds to the conclusion about periodical change of rates of growth crystal. In the limit case it may be connected with periodical change of growth mechanism: tangential $\rightarrow$ normal $\rightarrow$ tangential $\rightarrow$ normal...Theoretical model shows that alternation of growth rate are possible only under strong unequal conditions,corresponding with Prigogine's idea.Therefore one can make the conclusion that selected Siberian diamonds were growthed under strong intastable state.

6. Reference.

1.Aleksandrov L.N.,Gafitullina D.S.et.al.. Res.and Techn.Cryst.,v.17, n.11(1982)

2.Gafitullina D.S.,Solodova J.P. et.al. Dokladi AN SSSR, v.284, n.6 (1985).

3.Lang A.R. Pros.Soc., 278 K, 1373 (1974)

4.Ashurov M.Kh.,Gafitullina D.S. Procceding SPIE's,v.1550, 5054, (1991)

5.Cahn J.W.,Hillig W.B.,Sears G.W.. Acta Metal., 12, 1421 (1964)

6.Routburd A.L. In "Modern Problem of Crystalography", (Russian),p.345,(1975)

7.Shklowskii V.I. Usp.Phys.Nayk(Russian), v.157, n.2,(1989).